RESTRAINED SHRINKAGE BEHAVIOR OF POLYPROPYLENE FIBER REINFORCED SELF-CONSOLIDATING CONCRETE

By

ZEESHAN GHANCHI

A thesis submitted to the

Graduate School – New Brunswick

Rutgers, The State University of New Jersey

In Partial Fulfillment of the requirements

For the degree of

Master of Science

Graduate Program in Civil & Environmental Engineering

Written under the direction of

Dr. Hani H. Nassif

And Approved by

_____

_____

_____

New Brunswick, New Jersey

January 2015

ABSTRACT OF THE THESIS

RESTRAINED SHRINKAGE BEHAVIOR OF POLYPROPYLENE FIBER REINFORCED SELF-CONSOLIDATING CONCRETE

By ZEESHAN GHANCHI

Thesis Director:

Dr. Hani H. Nassif

Using self-consolidating concrete (SCC) in construction reduces labor and time requirements for concrete construction. With the advancement of chemical admixtures, such as high range water reducers, SCC mixes are stronger and more workable than ever before. As a result, SCC is becoming an increasingly viable option in the construction industry. Despite the improvement in chemical admixtures, many complications that arise in ordinary concrete are also prevalent in SCC. Concrete shrinkage, and by extension shrinkage-induced cracking, is one of the most common problems associated with the use of concrete.

This study addresses the issue of shrinkage-induced cracking on SCC observing the effects of ¼" (6.35mm) long polypropylene fibers mixed into the concrete. Using a low-cement SCC control mix, fibers are added at 0.10, 0.15 and 0.20% by volume to create three fiber-reinforced self-consolidating concrete (FRSCC) test mixes. The effects on slump flow and passing ability due to the addition of fibers are measured. AASHTO

PP 34 restrained ring samples are collected for each mix and, after a 24 hour moist cure, the stress development in the rings is monitored. Additional vibrating wire strain gauges (VWSGs) are partially embedded into the concrete in an attempt to directly measure concrete strain. Strength tests are conducted at 28 days and free shrinkage measurements are taken regularly by means of a length comparator.

Workability and, to a greater extent, passing ability suffered as a result of fiber addition. The addition of high-range water reducer (HRWR) alleviated the workability problems to an extent, however segregation and bleeding resulting from too much HRWR limits the upper threshold of fiber loading in SCC mixes.

Free shrinkage was improved by 9% and cracking strain increased by over 22% when fibers were added at 0.20% by volume. As a result, initial cracking in FRSCC restrained shrinkage rings was delayed by up to 9 days and maximum crack width was reduced from 0.085mm to 0.065mm.

The partially embedded VWSGs were able to measure strain development in individual segments of the concrete rings. They can provide information on where a crack may form without noticeably affecting the strength capacity of the ring.

ACKNOWLEDGEMENTS

I would first like to thank Dr. Hani Nassif for his support throughout my undergraduate and graduate studies at Rutgers. Dr. Nassif gave me the opportunity to prove myself as an undergraduate research assistant and working with him since then has been an honor.

I would like to thank Dr. Hao Wang for being on my committee. I would also like to thank Dr. Husam Najm for being on my committee as well as the guidance he has provided since my freshman year at Rutgers. Both inside and outside the classroom, Dr. Najm has made strived to make himself available to assist me and other students.

I would like to thank the undergraduate research assistants, Dalexander Gonzales, Zaina Hamdan and Giuseppe Liberti, for the countless hours of mixing, testing and crack-mapping. Without their help this work would have been impossible. I would also like to thank Adi Abu-Obeidah; since joining the research group, Adi's experience and knowledge has helped on every stage of this project.

I would like to thank Euclid Chemical, LaFarge, Holcim and Clayton Concrete for donating materials towards the completion of this study.

Finally, I would like to thank the RE-CAST University Transportation Center for funding my research as well as the Rutgers Civil & Environmental Engineering department.

TABLE OF CONTENTS

LIST OF TABLES

LIST OF FIGURES

CHAPTER I

1 INTRODUCTION

1.1 PROBLEM STATEMENT

Concrete is a versatile building material taking the shape of the form it is poured into. During the process of hardening, concrete undergoes a change in volume known as shrinkage. While restrained, the concrete's resistance to this shrinkage causes stresses to build up within the concrete that often results in shrinkage cracks. Over time, and with the help of outside factors including loading, temperature changes and freeze-thaw cycles, these cracks propagate and present a host of problems. On bridge decks, deicing salts and acid rain seep through these cracks and accelerate the deterioration of steel reinforcement and underlying steel girders. Repair costs built rapidly as the rust expands, accelerating the propagation of concrete cracks and creates a positive feedback loop. While there are a number of other factors that influence the cracking behavior of a concrete deck, including environmental effects, the magnitudes of loads and the concrete mix design, a reduction in shrinkage induced cracking provides many benefits towards the longevity of a concrete structure.

Shrinkage alone does not lead to cracks in concrete, but a combination of concrete shrinkage, restrained conditions and a low tensile strength combine to cause cracks. A

free unrestrained sample of concrete will experience a reduction the overall volume, but this shrinkage will not cause cracking because restraint is not present. Similarly, a restrained sample of concrete with high enough tensile stress will resist cracking even while shrinking. In a bridge deck, restraint can come from a number of sources included embedded rebar, decking studs, and steel girders. Additionally, restraint is not evenly distributed along the length of a concrete deck; negative moment regions and sections close to abutments are more prone to restrained conditions. While the sources of restraint are unavoidable, it is possible to reduce the amount of cracking by limiting the shrinkage of the concrete, increasing its tensile strength or both.

The concrete mix is a delicate balance of cementitious material, aggregate, water and chemical admixtures, each of which plays a role in the shrinkage and strength of concrete and therefore each affects the concrete's behavior under restrained conditions. It is therefore important to identify what role each material makes and what materials can be added or changed to reduce cracking.

Fibers are a common addition to concrete mixes, added in an effort to increase tensile strength and therefore increase the resistance to cracking. Common fiber materials include steel, polypropylene, glass and polyvinyl-alcohol (PVA). The addition of fibers into a concrete mix must be done in carefully measured amounts to reduce the risk of clumping or excessive loss of slump. When used correctly, fiber reinforced concrete can have lower shrinkage and less cracking to its conventional counterpart.

Additional measures can be taken after pouring to provide ideal conditions for concrete curing. A high humidity or fully moist environment can assist in the hydration

of cement and increase concrete strength while simultaneously reducing drying shrinkage.

By minimizing concrete shrinkage and limiting the formation of concrete cracks, a bridge deck can last longer and require less frequent repairs. As a result, congestion due to lane closures can be reduced and the lifetime cost of a project can be dramatically lowered. The first step to achieving this goal is to design a better concrete mix.

In an effort to find an improved concrete mix, the construction industry has increasingly utilized self-consolidating concrete (SCC) for their concrete mixes over the past few decades. SCC refers to a group of highly workable concrete mixes capable of filling voids and spaces within formwork without external compaction or vibration. SCC is characterized by its ability to retain a low viscosity without any segregation or bleeding. By eliminating or drastically reducing the need for vibration, concrete placement can be done faster and construction costs reduce as well. Combining these benefits with those of a low-shrinkage mix while keeping material costs down can result in a highly desirable and highly profitable concrete mix.

1.2 RESEARCH OBJECTIVES AND SCOPE

The purpose of this research is to analyze the restrained shrinkage properties of several fiber reinforced self-consolidating concrete (FRSCC) mixes. Materials will be gathered locally with overall cost in mind in order to achieve a mix that is both financially reasonable and structurally beneficial to those in the construction industry. Polypropylene fibers of ¼" length will be used in varying quantities. Polypropylene is a relatively inexpensive synthetic fiber that provides tensile strength improvements while

being flexible enough to allow SCC-like flow. Wet concrete properties will be observed closely to determine the affect the fibers have on flow. Additionally, mechanical properties will be tested including compressive strength, elastic modulus, tensile splitting strength, and free and restrained shrinkage. In total, four mixes will be texted with fiber contents, by volume, of 0.00%, 0.10%, 0.15% and 0.20%. Mixes will have a water-cement ratio of 0.425 and a total cementitious content of 675 lb/cu yd. Grade 120 ground granulated blast furnace slag (GGBFS) will be used at a replacement rate of 35%. Slag is an inexpensive locally sourced cementitious material that can provide additional strength and reduce bulk cost. Water reducing and air entraining admixtures will be used to achieve desired slump and air contents. Concrete properties will follow specifications set by the New Jersey Turnpike Authority (NJTA) for drill shaft concrete as no NJTA specifications are currently set for structural SCC.

1.3 THESIS ORGANIZATION

This thesis consists of five chapters as the following:

Chapter I serves as an introduction consisting of the problem statement, research objective and scope and thesis organization.

Chapter II covers the general background and literature review on the types of shrinkage, the factors contributing to shrinkage, SCC and polypropylene fibers, and similar work done as part of previous studies.

Chapter III covers the experimental program including the material properties and supplies as well as the mixing and testing procedures.

Chapter IV covers the results of the tests, including the mechanical properties, shrinkage tests, crack maps as well as certain strain calculations.

Chapter V covers the conclusions, recommendations and possible scope for future research.

CHAPTER II

2 LITERATURE REVIEW

2.1 INTRODUCTION

Fiber-reinforced self-consolidating concrete (FRSCC) is a relatively new area of concrete study that aims to simultaneously address two inherent issues with concrete, shrinkage cracking and consolidation requirements. Conventional concrete consists of a carefully measured proportion of water, binder, aggregate and occasionally chemical admixtures. Upon placement, this concrete requires compaction in the form of mechanical vibration or rodding to rid itself of air voids that cause structural inconsistencies. Over the course of a few hours, the concrete begins to harden in a chemical reaction process known as curing. As a result of this chemical reaction there is a net loss in volume, known to engineers as concrete shrinkage. In practical applications, this shrinkage causes stresses to build up within a concrete structure, eventually resulting in shrinkage induced cracking. Over the life of a structure, these cracks are prone to expansion and propagation due to various environmental factors including de-icing salts and temperature variations. Once sufficiently deep, the cracks expose the underlying steel reinforcement to the same environmental effects, accelerating their corrosion and further weakening the structure.

FRSCC aims to reduce the time involved in construction and minimize shrinkage cracking. An ideal FRSCC mix would require no compaction on placement, offer sufficient resistance to shrinkage cracking and meet the strength requirements of conventional concrete.

2.2 SELF-CONSOLIDATING CONCRETE (SCC)

Self-consolidating concrete, or self-compacting concrete (SCC), was first developed in the late 1980s by Professor Hajime Okamura in Japan. In an effort to offset the increasing shortage of skilled labor in Japan, the construction industry sought methods of reducing the labor requirements of construction projects. SCC was developed as a response to this growing need, it offered improved placement times and construction quality while reducing time and labor requirements (Okamura, Maekawa & Ozawa, 1993). Since then, SCC has grown in popularity around the world. While use in the United States has lagged behind, Europe and Asia were quick to adopt the technology, using it to construct several bridges in the early 2000s. Slowly, the U.S. precast industry has begun to apply SCC to architectural concrete and highway bridge construction projects (Tande & Mohite, 2007).

As SCC is characterized by its workability, it is important to understand what "workability" means and how it can be tested. The plastic properties that define SCC are its filling ability, passing ability and segregation resistance. Filling ability refers to the concrete's ability to fill formwork, as measured by the slump flow test. Passing ability refers to the ability of the concrete to pass through gaps commonly found between reinforcement bars; this is measured by the L box and J ring test. Finally, segregation

resistance refers to the concrete's ability to remain homogenous, keeping the aggregates from sinking and paste from floating to the surface, as indicated by the visual stability index (VSI) (Shindman & Panesar, 2012). Maintaining, and improving, all three properties while keeping a structurally strong concrete drives the research in concrete materials and admixtures.

Two basic concepts of SCC mix design have held true since the earliest developments. First, the volumetric ratio of paste in concrete must remain relatively high to allow the aggregates to flow smoothly as coarse aggregates have higher energy requirements to flow. Additionally, a lower water-paste ratio will help prevent segregation and bleeding, two undesirable effects in concrete. In the decades since its development, SCC has improved thanks to innovations in new materials including advanced chemical admixtures. Whereas the early SCC prototypes used conventional concrete materials, new superplasticizers and viscosity modifiers allow engineers to create a self-consolidating mix with high-performance properties (Okamura & Ouchi, 2003). Admixtures can also be used to address the issue of concrete shrinkage; shrinkage reducing admixtures and internal curing agents such as paraffin-based admixtures reduce the effects of drying shrinkage. Fibrillated polypropylene fibers and latex-based admixtures can also be added to improve shrinkage performance (Leemann, Nygaard & Lura, 2014). Some of these solutions may come at a high cost in bulk concrete applications so it is essential to determine the cost-effectiveness and the performance of each option.

Air entraining admixtures (AEA) are commonly found in concretes susceptible to freeze-thaw or placed in environments where temperature fluctuation can negatively

affect concrete. AEA disperses microscopic air bubbles within the mix during the process of mechanical mixing (Du & Folliard, 2005). As temperatures drop, water that has been absorbed into the concrete freezes and expands, exerting a great deal of stress on the crystalline structure. Without the microscopic air voids, the water would have no room to expand and cracks would form in the concrete. Because the bubbles added by AEA have a tendency to coalesce and combine, especially so in self-consolidating mixes, the amount of AEA must be carefully adjusted to reach the required air content (Barfield & Ghafoori, 2012).

In conventional concrete, water reducers are extremely beneficial in minimizing the water to cement (w/c, or water to binder, w/b) ratio which in turn results in a higher strength product (Nocun-Wczelik, Wasag, Styczynska & Miklaszewski, 2009). The admixtures allow for an increased slump with far less bleeding and segregation. As a result of having less water in the mix, large air voids resulting from the evaporation of excess water are reduced and permeability of the concrete member decreases. Some water reducers, also known as plasticizers, result in an excess amount of microscopic air voids and must contain anti-foaming agents. Viscosity modifying admixtures, or VMAs, are often used in conjunction with plasticizers to further reduce foaming and segregation in highly workable self-consolidating concrete mixes (Lazniewska-Piekarczyk, 2013). To maintain a high-strength, low w/c, workable SCC mix, the careful use of water reducers is essential. The additional benefits of durability and segregation-resistance make water-reducer a popular addition to all high-performance concretes.

In addition to ordinary Portland cement (OPC), the binder portion of a concrete mix may also include one of several pozzolanic cementitious materials. Pozzolans, such

as ground granulated blast furnace slag (GGBFS) or fly ash, increase the durability and strength of a concrete mix. GGBFS in particular, being a by-product of steel production, has been shown to increase 28-day strength of concrete significantly, and shows a greater increase in strength at later ages (Rajamane, Annie Peter, Dattatreya & Neelamegam, Gopalakrishnan, 2003). With sufficient curing, GGBFS, or slag, has the ability to decrease chloride ion penetration, increase resistance to sulfate attack and lower the permeability of the concrete. As with all pozzolans, slag reacts with the byproduct of cement hydration in what is known as a pozzolanic reaction (Osborne, 1999). Because the pozzolanic reaction occurs over a longer period of time, the overall heat generation of the hydration reaction in the early stages of concrete curing is reduced. In SCC, where cement content is relatively high, high temperatures result in evaporation of mixing water and as a result a higher w/c ratio is required to compensate (Khayat, 1999). The addition of slag can help reduce bulk cost and improve the overall quality of an SCC mix in an environmentally friendly manor.

While additives and admixtures alleviate many of the problems associated with concrete, some weaknesses of concrete are amplified in SCC mixes. Because of the higher cement content of SCC, shrinkage is often greater in SCC mixes. Under restrained conditions, higher shrinkage would result in more strain. When this strain exceeds the tensile stress of the concrete, shrinkage cracking occurs. While measures can be taken to reduce shrinkage, including adding shrinkage reducing admixtures (SRA) or ensuring proper curing, cracking will typically be higher in comparison to similar conventional concrete mixes (Loser & Leemann, 2009).

2.3 FIBER-REINFORCED CONCRETE

2.3.1 Fiber Types and Classifications

The origins of modern fiber-reinforced concretes date back to the early 1960s in a paper published by the American Concrete Institute. The authors observed the tensile strength in response to the addition of uniformly distributed short-length wire reinforcement (Romualdi & Mandel, 1964). Since then, fiber reinforcement has evolved in many ways including the addition of synthetic and natural fibers, recycled fibers, micro and nano-fibers, and new fiber shapes among many other discoveries. Presently, because of the wide range of research being done in fiber-reinforced concrete, work in the field must be targeted to a narrow scope.

Fibers can be categorized many different ways. Primarily, a fiber is defined by the material it is made of. The earliest concrete "fibers", tested in 1964, were metal wires cut and dispersed into concrete. Fifty years later, modern fibers have come a long way. Fiber materials include acrylic, aramid, carbon, nylon, polypropylene, cellulose and many other synthetic and natural materials. Fibers can be further classified by their geometry. The length, diameter, aspect ratio and denier (mass per 9000 meters of fiber) are commonly used classification properties. Because many fibers rely on the physical bond with concrete, the geometric properties of fiber play an important role in fiber performance. Additionally, the strength, toughness and many chemical properties including alkali-reactivity and melting point are used to classify fibers (Zollo, 1997). Choosing the best fiber for a particular application requires careful thought and knowledge of all of the proposed fiber material's properties.

2.3.2 Polypropylene (PPE) Fibers

Polypropylene as a material is a widely used plastic in various industries including electrical, chemical and automotice. As a fiber, Polypropylene (PPE) is an inexpensive synthetic option; it is believed to be among the most effective fiber materials in limiting the cracking of concrete. PPE fibers are effective in small dosages with improvements being detectible at 0.1% fiber volume. Studies show PPE fibers reduce total crack area, maximum crack width and the number of cracks. A higher fiber volume generally means improved cracking resistance. Longer fibers of a low denier and high aspect ratio are found to be more effective at reducing crack area and width. Finally, fibrillated fibers have been found to be more effective than their non-fibrillated counterparts in reducing plastic shrinkage (Banthia & Gupta, 2006). Polypropylene fibers are also effective in improving impact resistance and toughness of concrete materials. As a result, PPE-reinforced concrete structures are expected to have a longer service life. (Aslani & Samali, 2014).

The main drawback of fiber reinforced concrete is the decrease in workability and the problems associated with improper mixing such as fiber clumping and non-homogenous casting. Mixing with fibers often requires special care and an adequate slump to assure fibers have been evenly distributed. Fibers mixed into concrete increase the required energy for a workable concrete and can gather around blockages such as steel reinforcement and decrease passing ability greatly. Plasticizers and viscosity modifiers can be used to offset this problem to an extent, however too much plasticizer can lead to bleeding and segregation which leads to a poor overall concrete quality (Mazaheripour et al, 2011).

2.4 TYPES OF CONCRETE SHRINKAGE

Concrete shrinkage starts from the time right after concrete has been cast and continues long into a concrete structure's life. Shrinkage comes in various types, each the result of different chemical and physical reactions. Each type of shrinkage affects the concrete to varying degrees and may differ in magnitude depending on age and environmental factors. The types of shrinkage include plastic shrinkage, thermal shrinkage, autogenous shrinkage and drying shrinkage.

2.4.1 Plastic Shrinkage

Plastic shrinkage of concrete takes place early in the concrete's life, within the first few hours after casting. During this time, the concrete is still in its plastic stage and has yet to attain strength from hydration. The combination of low strength with plastic shrinkage makes the concrete susceptible to plastic shrinkage cracking (Dao, Dux, Morris & O'Moore, 2010).

Plastic shrinkage is caused by the evaporation of water from concrete while it is still in a plastic state. The evaporation of water causes an overall loss of concrete volume which results in shrinkage. Factors that increase the rate of evaporation lead to a higher amount of plastic shrinkage, including high temperatures, windy conditions and low relative humidity. Concrete slabs with a high surface-area-to-volume ratio are also subjected to higher plastic shrinkage (Mora-Ruacho, Gettu & Aguado, 2009).

In high performance concretes (HPC), where low water-cement ratios are often used, plastic shrinkage cracking is a major concern. Shrinkage reducing admixtures (SRA) has shown some improvement in plastic shrinkage cracking, as has the inclusion

of fibers and other admixtures (Mora-Ruacho et al, 2009). For most HPC applications, it is essential to begin wet cured immediately after pouring. By stopping the evaporation until the concrete has hardened, it is possible to reduce plastic shrinkage and eliminate plastic shrinkage cracking.

2.4.2 Thermal Shrinkage

Thermal shrinkage is shrinkage that is a result of thermal expansion and subsequent contraction of a concrete element. Certain materials in the concrete may make the concrete more susceptible to thermal shrinkage by increasing the concrete's thermal expansion coefficient (Mindess, Young & Darwin, 2002). Cycles of thermal stress are common in outdoor structures where temperatures vary throughout the day and throughout the seasons.

Thermal stress is also induced soon after casting. The exothermic hydration reaction that begins as soon as the water touches the cement increases the temperature of the mix well above ambient temperatures. The concrete stays at this elevated temperature as it is poured into formwork and around reinforcement bars. As the concrete sets and the reaction slows, the member cools, contracting slightly. This contraction induces thermal stresses and can cause cracks in the concrete. Additionally, uneven temperature and moisture gradients cause thermally induced stresses between layers of the concrete, potentially leading to cracking on the outermost layer (Klemczak & Knoppik-Wrobel, 2014).

As the hydration reaction is fundamental to concrete, all sources of thermal stress cannot be eliminated. The heat of hydration, however, can be limited through the use of

chemical or mineral admixtures. Concrete setting retarders act as an inhibiter, slowing the hydration reaction which in turn lowers the internal temperature of the concrete. This extends the time needed for the concrete to gain strength, but decreases the thermal shrinkage stress (Osipov, 1976). Alternatively, mineral admixtures, including cementitious materials such as GGBFS can reduce the heat of hydration. Because the reactants of the pozzolanic reaction are the byproducts of the cement hydration reaction, pozzolans take slightly longer to react and harden. This means that, initially, only the ordinary Portland cement portion of the binder is reacting, while the pozzolan cementitious materials are less reactive (Khayat, 1999) By slowing the rate of reaction through the use of inhibitors or pozzolans, it is possible to reduce the heat of hydration and reduce thermal shrinkage during the early age.

2.4.3 Autogenous Shrinkage

Autogenous shrinkage occurs when the cementitious material of a mix shrinks in volume without any change in mass. The loss in volume comes from hydrating cement particles forming a fine network of pores within the concrete. Through the capillary effect of water, these pores drain water from the larger capillaries created during the mixing of concrete. Without the addition of external water to fill the capillaries, the cement structure undergoes a similar process to drying shrinkage, called self-desiccation (Tazawa & Miyazawa, 1995).

When findings on autogenous shrinkage were initially published in 1940, the total autogenous shrinkage in structures at the time was very small. That is because concrete at the time had a much higher water-to-binder ratio, leaving excess water to fill the newly

formed capillaries. As admixtures advanced, lower water-to-binder ratios were used to create higher strength concrete, autogenous shrinkage became more and more significant (Tazawa & Miyazawa, 1995). Methods have been developed to lessen the impact of autogenous shrinkage including fully submerging the concrete (Tazawa & Miyazawa, 1995) or using internal curing methods by presoaking aggregate (Cusson & Hoogeveen, 2008), however in most large-scale applications both of these methods are impractical due to cost. Autogenous shrinkage will remain an issue in mixes with high cementitious contents and low water-to-cement ratios.

2.4.4 Drying Shrinkage

Drying shrinkage is the result of a decrease in concrete volume from the evaporation of water. Drying shrinkage is the longest lasting stage of shrinkage in concrete, possibly continuing over a year after casting. Because drying shrinkage is dependent on many different factors, including humidity, mix design, temperature and time of curing, long-term testing is essential to providing an accurate model to predict drying shrinkage (Gardner, 2004).

As the concrete sits and hardens, water that has filled the pores begins to evaporate. Cohesion between the remaining particles of water causes a negative pressure to act on the walls of the pores. The pores shrink as a result of this inward pore pressure and cause an overall loss in concrete length. Several solutions have been tested to reduce the impact of drying shrinkage on the concrete structure. For example, decreasing the number of pores by increasing their respective size results in less overall shrinkage even with a greater evaporation loss (Collins & Sanjayan, 2000). Alternatively, keeping a

longer wet cure would delay the evaporation until the pore walls gain sufficient strength to maintain their shape. Shrinkage reducing admixtures can also be used to decrease the mixing water's cohesive properties and allow for a smoother evaporation (Mora-Ruacho et al, 2009). Minimizing the impact of drying shrinkage is important for real-world applications where evaporation is an inevitable part of a concrete pour.

2.5 FACTORS AFFECTING SHRINKAGE

Each component mixed into concrete has an effect on the concrete's final properties. The processes involved in cement hydration are complex and isolating any one variable to measure the effect on shrinkage is a difficult task. While the effect a single factor can have on the total shrinkage is seemingly small, on the order of 10^-6 strains, any improvement is significant and can extend the life of a concrete structure. It is therefore important to identify what effect each material will have on the shrinkage of concrete and weigh the benefits

2.5.1 Cement & Water

Both the amount of cement and the water-to-cement (w/c) ratio of concrete play a large role in the shrinkage of concrete. As many shrinkage processes are a direct result of the hydration reaction, the relationship between cement and shrinkage has been thoroughly studied.

When isolated, cement and water form what is known as cement paste. The cement paste undergoes hydration, just as a concrete mixture would, and shrinks due to similar chemical and physical processes. A part of the overall shrinkage is associated

with the chemical reaction itself, in which the reactants have a greater volume than the products. This “chemical shrinkage” can be described by a series of chemical reactions that occur in different stages of cement hydration. While the resulting loss in volume from these reactions is small compared to the overall shrinkage of concrete, chemical shrinkage is closely related to other types of shrinkage (Tazawa et al, 1995). Most chemical shrinkage testing, as required by ASTM C1608, limits the testing period to 24-hours, even though cement hydration occurs well past this time period. Yodsudjai & Wang (2013) tested different types of cement in an effort to create an accurate model for predictions of chemical shrinkage at later ages. They found that different types of cement experience different chemical shrinkage behavior as a result of the different components. Higher tricalcium aluminate (C3A) and tetracalcium alumino ferrite (C4AF) contents result in a higher chemical shrinkage (Yodsudjai & Wang 2013).

Low water-to-cement ratios are essential to creating a high-performance concrete. With low water-to-cement ratios, however, concrete is susceptible to evaporation of water that is needed for hydration. This makes a concrete more vulnerable to autogeneous shrinkage (Tazawa & Miyazawa, 1995) and plastic shrinkage (Mora-Ruacho et al, 2009). For creating high-performance concrete with minimal shrinkage, external curing is essential.

Different cement additives or cementitious materials are used to increase strength, decrease cost or have an effect on other properties of concrete. Silica fume, for example, is a common fine cementitious material used in high-performance concretes. When added to concrete, silica fume has a tendency to increase early age shrinkage and increase the demand for water. While late-age shrinkage is relatively unchanged, high early age

shrinkage can cause cracking to develop before the concrete has developed enough strength (Whiting et al, 2000).

Blast furnace slag, or slag cement, is another cementitious material created as a byproduct of steel production. Slag is beneficial as its use reduces the need for CO2 producing Portland cement and it can be added to concrete in large quantities (Roy, D.M., 1999). The use of slag cement has drawbacks, however. Concrete with slag cement replacement are observed to have a higher free shrinkage strain and a greater amount of cracking. While this can be alleviated somewhat with the use of shrinkage reducing admixtures, the solution adds cost to a solution meant to be cost-effective (Kanda, T. et al 2014).

Modifications to slag cement are also made to improve the mechanical properties of the concrete. While slag cement concrete typically has a higher overall strength compared to a pure Portland cement mix, slag cement has a lower reactivity and therefore has a lower early age strength. As a result, activated slag cement has been created containing chemical activators of varying amounts to improve early age mechanical properties. However, activated slag is still limited in utility because the activators add cost and the shrinkage performance is degraded when compared to Portland cement mixes (Melo Neto, 2007).

Silica fume and slag are typically smaller in particle size than ordinary Portland cement. This size difference has been found to be a key component in the shrinkage behavior of different concretes. As a cement particle is larger, the particle may not hydrate completely during concrete curing. The unhydrated portion of the particle acts as a restraint against shrinkage having a similar effect as aggregate particles. Therefore

coarse cement particles would lead to a lower overall shrinkage but a less complete hydration (Klieger & Lamond, 1994).

2.5.2 Aggregates

In high performance concretes, aggregates make up a majority of the concrete's volume. It is therefore no surprise that aggregates play a large role in the shrinkage and cracking characteristics of a concrete mix. Aggregates significantly affect the mechanical properties of concrete; they provide much of the strength and are the reason concrete often breaks in a characteristic brittle failure (Eldin & Senouci, 1993). The amount, type and size of the aggregates used have been shown to be an indirect cause of much of the shrinkage problems associated with concrete. While aggregates themselves do not shrink while the concrete cures, their rigidity and strength can prevent excessive cracking in concrete (Carlson, 1938).

Aggregates can also be used to mitigate shrinkage in other ways as well. Lightweight aggregates, though generally weaker and less brittle than their heavier counterparts, are typically more absorbent. By soaking the aggregates in water, lightweight aggregate has been shown to decrease the self-desiccation of concrete that causes autogenous shrinkage. Water that is lost through self-desiccation is replaced by water from the lightweight concrete. This can be effective with just a partial replacement of conventional aggregate with presoaked lightweight aggregate (Bentur et al., 2001). Because of the internal water's affect on concrete shrinkage, it is also important to assure each mix has identical moisture content values as the shrinkage behavior may change even if the water-to-cement ratio is identical.

2.5.3 Chemical Admixtures

Admixtures come in liquid or solid form and are added to concrete in order to change the mix's properties. Over the past decades, dozens of new admixtures have been created to change almost any of the properties of concrete including entrained air, workability, setting time, permeability, and color (Kosmakta & Wilson, 2011).

In high performance self-consolidating concrete, water-reducing admixtures are necessary to maintain flowability while reducing water-cement ratio. Because the water-reducing agents are added to a mix with low water-to-cement ratio, the mix is more susceptible to autogenous shrinkage. To some extent, it has been shown that water reducers can offset the plastic state shrinkage that low water-to-cement mixes typically have. This effect is dependent on the type and amount of water reducer added, but polycarboxylate water reducers have been found to be more effective (Gen Quin et al, 2012).

To further offset the effects of shrinkage, shrinkage reducing admixtures (SRAs) can be added to a mix. SRA works to decrease shrinkage in such a way that does not depend on expansive reactions such as those caused by type-K cements. SRAs mix with the water and decrease surface tension on the pore water. Normally, the evaporation of pore water causes an inward collapse of a pore because of the cohesive properties of water. With SRA, the pore water evaporates slowly and the pore walls remain intact. As a result, shrinkage is decreased and restrained shrinkage cracking is markedly reduced (Folliard & Berke, 1997). While SRAs are beneficial in reducing concrete shrinkage, their cost inhibits their adaptation on large-scale projects. Alternative solutions, such as an optimized mix design, are often preferred.

2.5.4 Fibers

Fibers are included in high-performance concretes because of their high-strength qualities. The high tensile strength combined with the high length-diameter ratio allows them to provide mechanical resistance to pullout. This pullout resistance means crack widths are decreased and longitudinal propagation is reduced (Saje et al, 2011).

The improvement of a concrete's properties is highly dependent on the type of fiber being used. Natural fibers, for example, may be more economical but produce a lower modulus of elasticity and do not bond to the concrete matrix as well as other fibers. Therefore natural fibers do not generally perform as well as synthetic and metallic fibers. Steel fibers, on the other hand, are highly effective in improving strength but often need to be added in large quantities. The long, stiff, steel fibers may inhibit flow and make uniform distribution exceptionally difficult (Shah, 1981). Polymer fibers, such as polypropylene or nylon, are used because, in addition to adding tensile strength, the fibers offer resistance to impact blows and plastic shrinkage cracking. While polymer fibers may complicate the mixing process and make dispersal difficult, the benefits they provide can greatly improve concrete's lifespan (Song et al, 2004).

2.5.5 Environmental Factors

Because most shrinkage processes are a function of evaporation, the climate and environmental conditions of concrete are critical in minimizing shrinkage. In general, a higher temperature increases the rate of evaporation and leads to a higher early autogenous shrinkage but a lower later-age drying shrinkage. Low temperatures generally lead to the opposite result. However both scenarios are not equal. Because autogenous

shrinkage occurs when the concrete is at a greater risk of cracking, high temperatures generally lead to more cracking in concrete. Some of this effect can be mitigated through sufficient wet curing, but environmental conditions should still be factored in before beginning a concrete pour (Chu et al, 2012).

Adequate humidity can simulate a complete wet cure sufficiently enough to decrease shrinkage cracking. By keeping newly poured concrete under humid conditions, strength gains increase and evaporation decreases (Qian et al, 2006). The combined effects decrease shrinkage cracking. It is therefore important to ensure that, in addition to temperature, humidity is kept consistent throughout shrinkage testing.

2.6 RESTRAINED SHRINKAGE TESTING

The restrained shrinkage ring test is a standard implemented by the American Association of State Highway and Transportation Officials (AASHTO). The test is typically used for comparative studies to determine the difference in cracking behavior between two mixes. Compared to similar testing methods that apply active restraint to simulate internal stresses in curing concrete, the ring test is simple to set-up and low cost making it more approachable as a research tool and also a viable option for quality control testing. The test, however, is not designed to give quantitative information on stress development or predict cracking behavior in real-life situations.

To use the data gathered from the ring test in a more practical setting, Hossain & Weiss published a study on the assessment of stress development in restrained ring specimens (2004). In their study, they found that, using the strain in the ring and the known geometric dimensions of the steel, and equation could be developed to calculate

the residual stress in the concrete. The relationship they found is shown below in Equation 2.1 (Hossain & Weiss, 2004).

$$\sigma_{actual} = -\varepsilon_{steel}(t) * E_s * C_{3r} * C_{4r} \quad (2.1)$$

$$\varepsilon_{steel}(t)\ is\ the\ strain\ in\ the\ steel\ at\ time\ t$$

$$E_s\ is\ the\ elastic\ modulus\ of\ steel$$

$$C_{3r} = \frac{R_{OS}^2 + R_{OC}^2}{R_{OC}^2 - R_{OS}^2}$$

$$C_{4r} = \frac{R_{OS}^2 - R_{IS}^2}{2R_{OS}^2}$$

$$R_{OS}\ is\ the\ outer\ radius\ of\ the\ steel\ ring$$

$$R_{IS}\ is\ the\ inner\ radius\ of\ the\ steel\ ring$$

$$R_{OC}\ is\ the\ outer\ radius\ of\ the\ concrete\ ring$$

The American Society of Testing and Materials (ASTM) has released their own standard for a restrained shrinkage test. The ASTM ring differs slightly in geometry from the AASHTO test. The AASHTO ring measures 0.5 inches (12.7mm) thick, 6 inches (152mm) high and 12 inches (305mm) in outer diameter with a total concrete thickness of 3 inches (76mm) all around. The ASTM ring, on the other hand, measures 0.5 inches (13mm) thick, 13 inches (330mm) outer diameter and 6 inches (152mm) in height. The wall thickness for the ASTM test is 1.5 inches (38mm). Since the ASTM test uses a larger diameter ring and a smaller thickness concrete, cracking is expected to occur earlier and be more extensive. For larger aggregate, however, it is recommended to use

the AASHTO ring test because of the 3 inch concrete thickness. For mixes with lower drying shrinkage, cracking may not occur at all with the AASHTO ring test and modifications would need to be made to induce cracking.

2.7 SUMMARY OF WORK PERFORMED BY OTHERS

2.7.1 Mechanical Properties of SCC & FRSCC

The inclusion of fibers in concrete is known to provide mechanical resistance to flow and reduce the workability of SCC. El-Dieb and Taha extensively studied these effects and conducted a study to find the degree to which the addition of fibers can affect the flow of SCC. Working with polypropylene fibers, they concluded that the relationship between fiber volume and flow characteristics was directly proportional and dependent mostly on the fiber volume and the cement content. After setting a threshold, below which a concrete could not be categorized as SCC, they found that the flow properties of SCC were affected beyond a usable threshold when fiber volume began to exceed approximately 1,300 g/m^3 (2.2 lb/yd^3) (El-Dieb & Taha, 2011).

Once cured, fiber reinforced concrete is expected to significantly improve mechanical properties when compared to conventional concrete by way of increased tensile and flexural strength. The fibers are also expected to offer additional cracking resistance. Gencel et al. conducted a study to measure the effects of polypropylene fibers on the mechanical behavior of concrete. Using high cement contents and a wide range of fiber contents, they tested FRSCC's unit weight, compressive strength, splitting tensile strength, flexural strength, pulse velocity and modulus of elasticity. Throughout the scope of the experiment, they found that the strength of concrete increased with the utilization

of higher fiber content. Tensile and flexural strength was impacted the most in comparison to compression strength and the elastic modulus, which showed somewhat smaller improvements (Gencel et al, 2011).

2.7.2 Shrinkage Properties

While improvements in tensile and flexural strength will limit the size of concrete cracks, improving shrinkage performance is an essential factor for stopping the initial formation of cracks. In 2011, Saje et al. evaluated the impact of various amounts of polypropylene fibers on the shrinkage behavior of high performance concrete. To quantify the improvement, measurements of concrete shrinkage were taken using embedded transducers immediately after hardening. By testing batches of concrete with increasing quantities of polypropylene fibers, the study concluded that shrinkage of fiber-reinforced concrete could be reduced by increasing the fiber content up to 0.5% by volume. They noted that after 0.5% fiber volume, the improvement in shrinkage was negligible. The study also found that workability decreased significantly upon reaching 0.25% fiber volume (Saje et al, 2011). Maintaining a balance between shrinkage reduction and workability is crucial for an FRSCC mix.

2.7.2.1 Restrained Shrinkage Ring Tests

Observing the shrinkage behavior of fiber reinforced concrete is important, but it does not give a complete understanding of the development and propagation of shrinkage induced cracking. The concrete ring test is used as a method to compare different concrete mixtures by observing the formation of cracks as concrete shrinks around a steel ring. Hossain and Weiss used this test to observe the stress development in mortar mixes

subjected to restrained shrinkage. They found that the restrained shrinkage test can be used, not only as a comparative test, but also to quantify the buildup of stress by using strain gauges attached to the steel ring (Hossain & Weiss, 2004).

Turcry et al. used the restrained shrinkage ring test to investigate the specific cracking tendencies of SCC. To compare the results, three SCC mixes were paired with three ordinary concrete mixes designed with the same ingredients. By making only minor changes to the mix design, they found that the shrinkage cracking tendency is roughly equivalent provided the compressive strength is equal and segregation is not present in the SCC (Turcry et al, 2006).

While fibers are known to improve the mechanical properties of concrete, the effect it has on the restrained shrinkage behavior is more complex. Shah and Weiss (2006) looked at the affect fibers had on the restrained shrinkage of conventional concrete. Having established a method to determine the approximate residual stresses along the inner surface of the ring, the study used the same ring test to observe the changes in cracking behavior due to the addition of fibers.

In contrast to previous studies on stress development in rings which used nearly-homogenous mortar mixes, the addition of fibers adds a layer of complexity because of the unpredictable distribution of fibers within a mix. To better understand the effect this heterogeneousness has on the cracking behavior, Shah and Weiss (2006) utilized acoustic emission measurements, designed to detect microcracking before they appear on the surface of the ring.

The study found that fiber reinforced mixes developed stresses at a similar rate to non-fiber reinforced mixes provided free shrinkage was consistent. While the rate of

stress gain was similar specimens with a higher fiber volume tended to develop initial cracking at higher overall stresses, due to the increased tensile stress of fiber reinforced mixes. The authors noted that the acoustic activity of the non-fiber reinforced specimen plateaued prior to cracking and immediately fell as the crack formed. For the fiber reinforced mixes, the acoustic energy increased even as microcracking occurred beneath the surface of the ring. This indicated that the fibers used in the study bridged the gaps created by microcracking and the concrete still held some stress. These findings were corroborated by the steel strain gauges which found that higher fiber volumes permitted higher stresses in the ring before visible cracking developed. While small decreases in strain indicated the occurrence of microcracking, the fibers prevented the complete propogation of these cracks. Visible cracks in fiber reinforced mixes were also found to be of narrower width than those on the non-fiber reinforced specimen (Shah & Weiss, 2006).

This behavior has also been evaluated in a study published by Kwon et al. in which restrained shrinkage rings were used as a comparative test for four mixes of polypropylene and steel FRSCC. The testing in the study began by evaluating the flowability of FRSCC made of different fibers. They found steel fiber reinforcement hindered the flowability and passing ability much more than polypropylene fibers added at the same concentration.

Ring specimens were cast for the study measuring two inches thick and 16 inches in (outer) diameter. The narrow width, combined with only a one-day curing period, ensured all samples would crack even at fiber volumes of up 1.5%. As cracks formed, the steel strain as well as the crack width was observed. Strain and shrinkage data gathered

from the restrained shrinkage and free shrinkage tests was used to model the restrained shrinkage test in a finite element analysis (FEA) program(Kwon et al, 2007).

Kwon et al. found that while steel fiber reinforcement hindered the flowability of concrete more than polypropylene fibers, the cracking resistance was noticeably greater. They also found that the forces required to pull out fibers from the concrete decreased crack propagation and led to smaller, more evenly distributed, cracks. Even after the initial crack formed, fibers, especially steel fibers, managed to create a confinement effect by bridging the gap and preventing complete pullout. Steel fibers had an added benefit of reducing free shrinkage strains which is believed to have led to a further decrease in crack width when compared to polypropylene FRSCC cracks. The confinement effect was clearly visible in the restrained shrinkage steel strain graphs which showed smaller drops in stress from cracking and a reduction in stress loss due to cracking (Kwon et al, 2007).

Using the findings of previous researchers, this study aims to find an economical, effective FRSCC mix design that balances workability, strength and shrinkage resistance. The goal is to find the optimal fiber loading to minimize shrinkage cracking while working with a mix with low cementitious content.

The findings in Hossain and Weiss' study (2004) are based on using strain from the inner surface of the steel ring. While this is a good indication of the cracking potential of the material being tested, it is common for restrained shrinkage rings to exhibit uneven stress development. Strain measurements on different parts of the ring can show different value indicating that shrinkage may not be occurring evenly. Embedded strain gauges

inserted directly into the concrete may give us a better understanding of the behavior of concrete as shrinkage is occurring.

CHAPTER III

3 EXPERIMENTAL SETUP

3.1 INTRODUCTION

The experimental program for this study will include mixing concrete, casting samples, and performing various tests. Tests will include those done on plastic (wet) concrete, including slump, j-ring, unit weight, air content and visual stability index tests as well as those performed on hardened concrete, including compressive and tensile splitting strength, elastic modulus, and free and restrained shrinkage. Properties of the aggregate including absorption, specific gravity and moisture content are tested to ensure uniformity between batches. In total, four mixes are used in this experiment with two variables. The fiber content is increased between mixes and compensatory amounts of high-range water reducer (HRWR) are added to reach desired workability requirements. Testing is done according to ASTM and/or AASHTO specifications where applicable.

3.2 MATERIAL PROPERTIES

Materials used for mixing are obtained from various suppliers. Efforts are made to ensure materials could be made available locally as the final product is intended for use by local transportation agencies. Aggregates, both fine and coarse, are obtained from

Clayton Concrete in Edison, NJ. Grade 120 slag is provided by Holcim from their facility in Camden, NJ. Portland cement is supplied by LaFarge in Whitehall, Pennsylvania. Admixtures, including chemical admixtures and polypropylene fibers, are provided by Euclid chemical from East Brunswick, NJ. The material and supplier summary is shown in Table 3.1.

Table 3.1 Materials and Suppliers

Material	Type	Supplier
Cement	Portland Type I	LaFarge
GGBFS	Grade 120	Holcim
Fine Aggregate	Concrete Sand	Clayton Concrete
Coarse Agggregate	#8 (3/8”) granite	Clayton Concrete
Fibers	Polypropylene 1/4"	Euclid Chemical
Water Reducer	Plastol 5000	Euclid Chemical

Aggregate properties were tested prior to mixing. Sieve analysis on both types of aggregate is done according to ASTM C136. Coarse aggregate properties, including density, specific gravity, absorption and moisture content were tested using the procedure outlined in ASTM C127. The same properties for the concrete sand were found using ASTM C128. Results of these tests are outlined in Table 3.2.

Table 3.2 Coarse and Fine Aggregate Properties

Properties	Fine Aggregate	Coarse Aggregate
Specific Gravity	2.62	2.83
Fineness Modulus	2.35	6.03
Absorption	1.10%	0.40%
Moisture Content (batch)	0.47%	0.20%

Type I Portland cement is tested by the manufacturer to assure it meets all requirements set by ASTM C150 including chemical composition, physical properties,

reactivity and strength requirements. Similar requirements are outlined in ASTM C989 for the slag cement used. Manufacturer testing assures that all grade 120 slag meets the reactivity and other requirements set by ASTM standards.

Polypropylene fibers used in this study comply with ASTM C1116 and ASTM D7508 standards. The manufacturer provides fiber length, denier, and chemical and physical properties are provided by the manufacturer. The properties of the fibers are outlined in Table 3.3.

Table 3.3 Polypropylene Fiber Properties

Material	Monofilament Polypropylene
Specific Gravity	0.91
Length	1/4”
Melting point	320°F (160°C)
Denier	15

The high-range water reducer is tested by the manufacturer. The requirements of ASTM C494 Type F – High range water reducing as well as those of AASHTO M194 Type F and ASTM C1017 are all met by the manufacturer.

3.3 MIX PROPORTIONS

A total of four concrete mixes are prepared for this experiment. The proportions of these mixes are based heavily on the findings of a previous study conducted by the Virginia Transportation Research Council (Brown et al, 2008). All samples for each mix were cast from a single batch to ensure uniformity. The mix proportions are summarized in Table 3.4.

Table 3.4 Mix Proportions

Mix	PPE 0.00	PPE 0.10	PPE 0.15	PPE 0.20
Type I Cement, lb/cu yd	439	439	439	439
Grade 120 Slag, lb/cu yd	236	236	236	236
Total Cementitious	675	675	675	675
Water, lb/cu yd	287	287	287	287
W/C Ratio	0.425	0.425	0.425	0.425
#8 Coarse Aggregate, lb/cu yd	1436	1436	1436	1436
Fine Aggregate, lb/cu yd	1436	1436	1436	1436
High-Range Water Reducer, oz/cu yd	68	81	81	95
Fiber % by volume	0	0.1	0.15	0.2

In an effort to isolate variables, mix proportions are kept identical in all four mixes. Each mix contains 675 lb/cu yd of cementitious material, 35% of which is Grade 120 blast furnace slag and 65% of which is Type I Portland Cement. A water to cement ratio of 0.425 is targeted with a tolerance of +/- 0.02. Equal amounts of fine and coarse aggregate is used in the mixes, a total of 1,436 lb/cu yd of each, meaning the coarse-to-fine ratio is 1:1.

Fiber volume is varied between mixes, beginning with the control mix, PPE 0.00, having no fibers and mixes PPE 0.10, PPE 0.15 and PPE 0.20 having 0.10, 0.15 and 0.20 percent fiber by volume. As a result of the addition of fibers, workability is expected to decrease. To compensate for the loss in workability, small amounts of water reducer are added to the fiber-reinforced mixes in addition to the 68 fl oz/cu yd added to the control mix. Mixes PPE 0.10 and PPE 0.15 contain 81 fl oz of high-range water reducer per cubic yard and mix PPE 0.20 contains 95 fl oz/cu yd.

3.4 MIXING AND SAMPLING

The mixing, sampling and SCC testing procedure follows that done previously by El-Khoury (2010). Mixing and casting of samples is done according to ASTM C192 using a 6 cubic foot capacity electric mixer. Because of the sensitive nature of shrinkage testing, it is important to ensure all plastic and hardened state tests can be done from a single batch of concrete; therefore, each batch consists of approximately 3 cubic feet of concrete. The procedure for each test as well as the respective standard that was followed, when applicable, is briefly discussed in the following section.

3.4.1 Mixing (ASTM C192)

Figure 3.1 Mixer used for Mixing Samples

Prior to mixing, approximately 3 cubic feet of concrete are pre-batched into 5 gallon buckets to be used for mixing. The mixer used for this part of the experiment is shown in Figure 3.1. Materials for all four mixes are batched and prepared beforehand to expedite the mixing process.

The materials are added to the mixer separately with intervals of mixing in between. Prior to putting any of the materials into the mixer, the high-range water reducing admixture is mixed into the mixing water. The coarse aggregate is added first, followed by part of the mixing water and then the fine aggregate. The cement is then added and the remaining mixing water is added to the mixer. If needed, the polypropylene fibers are added to the mixer After the final mix interval, the concrete is ready to be used for plastic concrete tests.

3.4.2 Slump Flow Test (ASTM C1611), T20 & Visual Stability Index (VSI)

Because the mixes in this study are highly workable self-consolidating concrete, the standard slump test, ASTM C134, is not applicable. Instead, ASTM C1611 standards are followed to measure slump flow. The standards use identical slump cones, strike-off rods and base plate; however ASTM C1611 measures horizontal flow as opposed to vertical slump.

Figure 3.2 ASTM C1611 Slump Setup

The slump cone is filled with concrete and is lifted steadily to a height of 9 inches. A timer is used to measure the elapsed time between the lifting of the cone and the time the slump flow passes the 20-inch diameter circle marked on the base plate. This is the T20 time.

When the concrete has stopped flowing, the largest diameter of the resulting flow is measured along with the diameter approximately 90 degrees offset from the largest diameter. These two measurements are averaged and taken as the slump flow.

Before clearing the base plate, the slump flow is observed for any signs of segregation or bleeding. An index of 0 would be given to a concrete mass showing no evidence of bleeding or segregation. A VSI of 1 is given when slight bleeding is visible in the form of sheen on the concrete. When a slight mortar halo appears around the edges

of the slump flow, less than half an inch in thickness, a VSI of 2 is given and the concrete deemed unstable. If the halo exceeds half an inch in thickness or a pile of aggregate is visibly segregated in the center of the slump flow, a VSI of 3 is assigned and the concrete deemed highly unstable.

3.4.3 J-Ring Test (ASTM C1621)

The J-ring test is used to determine the passing ability of a self-consolidating concrete sample. The test is done using the procedure outlined in ASTM C1621. In addition to the slump cone, base plate and strike-off rod used in the slump flow test, a 16-bar, 12 inch diameter, metal J-Ring, as shown in Figure 3.3, is used for this test.

Figure 3.3 ASTM C1621 J-Ring

The slump cone is filled and lifted as it was in the slump test. When the concrete has stopped flowing, the largest diameter of the resulting flow is measured, along with the diameter 90 degrees offset from the largest. These two values are averaged to calculate the J-ring flow. The J-ring value is compared to the slump flow value to determine the blocking assessment. A difference of less than 1 inch indicates no significant blocking of the flow. If the difference is between 1 to 2 inches, minimal blocking may be occurring. Slump flow to J-ring difference of greater than 2 inches indicates extreme blocking.

3.4.4 L-Box Test

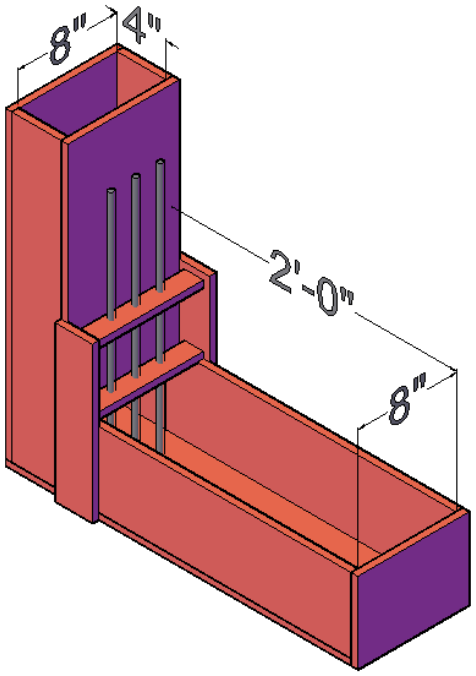

Figure 3.4 L Box used for Passing Ability Test

As no ASTM standards currently exist for the use of the L-box test, it has been used in this study as a comparative measure for passing ability. The box used, pictured in Figure 3.4, consists of a 24 inch high, 4-by8 inch shaft with a hole measuring 8-by-6 inches at the bottom. The gate covering the hole leads to a 24 inch long, 8 inch wide tray onto which the concrete flows. Before flowing into the tray, the concrete passes through three, evenly spaced (2" center-to-center), #3 steel reinforcement bars placed into the holes shown adjacent to the gate.

For this test, concrete is scooped into the top of the shaft and allowed to fall to the bottom while the gate is down. Once the shaft has been filled, the concrete sits for one minute and is then leveled without the use of any compaction or vibration. The gate is then lifted and the concrete is allowed to pass through the rebar and onto the tray. After the flow has stopped, a height measurement of the concrete flow is taken at the wall at the gate opening, h1, and at the opposite end of the tray, h2. The ratio of these two heights, h1/h2, is taken and compared between mixes to see the performance of each mix in a confined space.

3.4.5 Pressure Air Content Test (ASTM C231)

Figure 3.5 ASTM C231 Type B Pressure Air Meter

A type B pressure air meter is used to determine the air content of the concrete mixes. The meter, pictured in Figure 3.5, conforms to ASTM C231 standards. The pressure air test is done immediately after the slump test, provided the mix achieves the required workability.

3.4.6 Unit Weight and Gravametric Air Content (ASTM C138)

The unit weight, yield and gravimetric air content are measured using the procedure dictated by ASTM C138 standards. The test uses the same measuring bowl used for the pressure air content. By weighting the known quantity of the concrete, the test allows us to calculate concrete density and the air content by means of the gravimetric air content test. Knowing the theoretical density of the components and the

actual density of the concrete, the difference in the two values is due to the entrainment of air within the concrete.

Figure 3.6 ASTM C138 Unit Weight Measure

3.4.7 Sampling (ASTM C172)

Each mix is made in one batch with enough concrete to fill all of the required samples. Samples include two free shrinkage prisms measuring 3 x 3 x 10 inches, two AASHTO PP-34 specification restrained shrinkage molds with an inner concrete diameter of 12 inches, an outer concrete diameter of 18 inches and a height of 6 inches, and at least eight 4 x 8 inch cylinder molds for strength testing. The molds prepared for one mix are shown in Figure 3.7. No consolidation is used for filling samples as a self-consolidating mix is used in this study.

Figure 3.7 Molds Prepared for Sampling from 1 Mix

3.4.8 Curing and Storage

Samples are wet-cured for 24 hours while in their molds. A one-day wet cure is selected in order to match the specifications of the AASHTO PP-34 restrained shrinkage ring test. Free shrinkage and strength results are used as part of the restrained shrinkage calculations. To ensure a constant temperature, samples are placed in an environmental chamber kept at a constant 74 degrees Fahrenheit and 50% relative humidity. To keep the samples wet, layers of wet burlap are placed atop the samples and a polyethylene sheet is placed over top the burlap to keep evaporation to a minimum. After 24 hours, the samples are demolded, paraffin wax is used to coat the top surface of the restrained shrinkage

molds, the strain gauges are wired to a datalogger, and the uncovered samples are left in the environmentally controlled chamber until they are used for testing.

(a)

(b)

Figure 3.8 (a) Environmental Chamber and (b) Ring Sample Storage

3.5 LABORATORY TESTING

Laboratory testing is done at all stages of the study. Material information that cannot be gathered accurately from suppliers or manufacturers but is deemed necessary for the purposes of the study is tested using laboratory equipment. Prior to mixing, aggregate properties are tested including specific gravity, absorption and sieve analysis. This information is used when designing the concrete mixes. Plastic concrete tests are done immediately after mixing of the concrete. After testing and sampling is done,

additional tests are performed on hardened concrete throughout the testing period and presented in Chapter 4. The summary of all tests performed for this study is given in Table 3.5.

Table 3.5 Laboratory Test Overview

Test	Number of Specimens	Applicable Standard	Age of Concrete at Test, days
Sieve Analysis	1	ASTM C136	N/A
Specific Gravity, Absorption, Coarse	2	ASTM C127	N/A
Specific Gravity , Absorption, Fine	2	ASTM C128	N/A
Slump, T20, VSI	1	ASTM C1611	0
J-Ring	1	ASTM C1621	0
L – Box	1	N/A	0
Pressure Air Content	1	ASTM C231	0
Unit Weight	1	ASTM C138	0
Compressive Strength	3	ASTM C39	28
Tensile Splitting	3	ASTM C496	28
Modulus of Elasticity	2	ASTM C469	28
Restrained Shrinkage	3	AASHTO PP34	1 through 56
Free Shrinkage	2	ASTM C157	1 through 56

3.5.1 Sieve Analysis of Fine and Coarse Aggregate (ASTM C136)

Figure 3.9 Sieve Shaker and Sieves used for Sieve Analysis

Sieve analysis for both fine and coarse aggregate is done according to ASTM C136 standards. Samples of each aggregate used are collected, dried, measured and sieved using a set of metal sieves and a mechanical sieve shaker. The gradation of the materials used in this study will have an effect on the wet and cured properties of the concrete. The summary of the sieve analysis findings are shown in Table 3.6.

Table 3.6 Chart of Percent Passing for Sieve Analysis

Sieve	Sieve Opening Size, in	Percent Passing (Coarse)	Percent Passing (Fine)	Percent Passing (Combined)
3/8”	.375	85.70	100	92.85
No. 4	.187	7.11	99.36	53.24
No. 8	.0937	0.93	95.29	48.11
No. 16	.0469	0.82	84.01	42.42

No. 30	.0234	0.80	60.48	30.64
No. 50	.0117	0.78	22.51	11.64
No. 100	.0059	0.57	3.33	1.95
No. 200	.00295	0.45	0.19	0.32

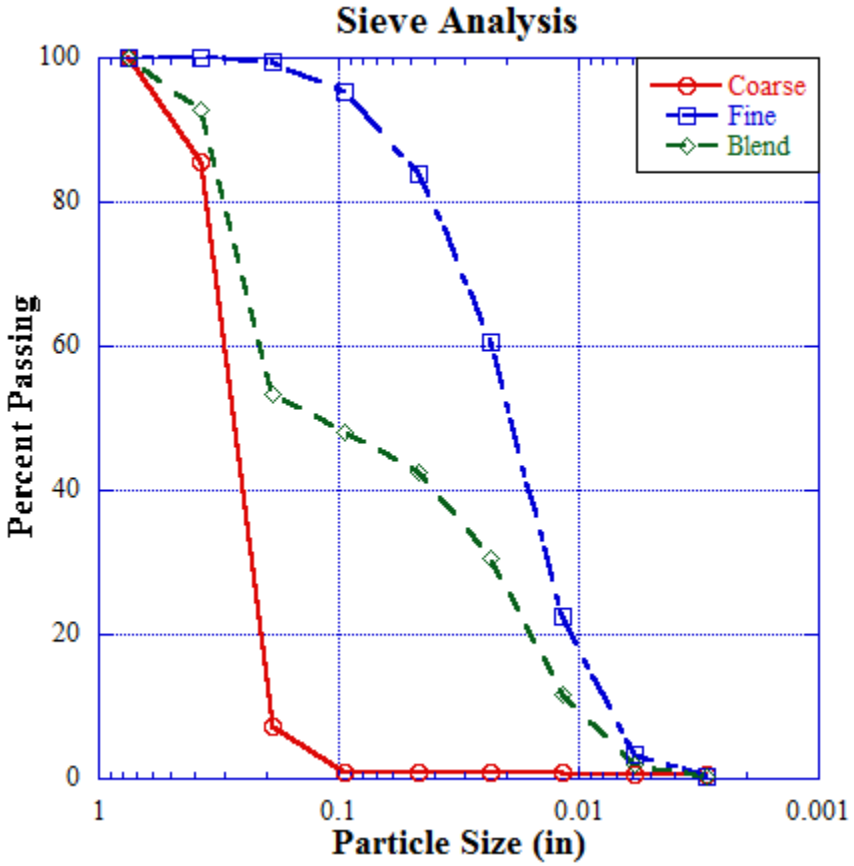

Figure 3.10 Seive Analysis Gradation Curves for Fine and Coarse Aggregates and Aggregate Blend

Fineness modulus can be calculated using the values of the cumulative percent retained on each of the sieves, from No.100 to 3/8", and dividing the sum by 100. The fineness modulus for the coarse aggregate is calculated to be 6.03, for the fine aggregate, 2.35, and for the combined blend, 4.19.

3.5.2 Specific Gravity and Absorption of Coarse Aggregate (ASTM C127)

The specific gravity and absorption test for coarse aggregate is needed to accurately measure the amount of coarse aggregate being added to the mix. The test is repeated every time a new batch of aggregate is brought from the supplier. For this test, a sample of oven dried aggregate weighing about 2kg is taken and, after cooling for approximately 1-3 hours, is immersed in water for 72 hours. The sample is removed from the water and rolled on an absorbent cloth until the surface is clear of visible films of water. The mass of the saturated surface-dry aggregate is taken and the sample is then immersed in water and the mass of the aggregate in water is taken. The water used for immersion is approximately 74 degrees Fahrenheit. The sample is then removed and placed in an oven for 3 hours and the dried aggregate mass is taken.

3.5.3 Specific Gravity and Absorption of Fine Aggregate (ASTM C128)

Just as with the coarse aggregate, the specific gravity and absorption of the fine aggregate needs to be tested to determine the correct amount of mixing water to add and to accurately measure the volume of the mixed concrete. This test is done prior to using a new batch of fine aggregate. To begin, a sample of aggregate is oven dried to a temperature of about 230 degrees Fahrenheit. After being allowed to cool, the sample is immersed in water for a period of 24 hours. The water is then decanted with care being taken to avoid loss of fines. The sample is then spread across a nonabsorbent surface and air-dried into a saturated surface-dry state. At this point, the sample is free flowing; to test for saturated surface-dry conditions, use the conical mold with the large diameter down and add sand until the mold is filled. Use the tamping rod and drop the rod 25 times

from approximately 5mm above the surface. After loose sand is removed from the base of the cone, the cone is lifted. If the sand holds its shape, surface moisture is still present; if the sand slumps slightly, the aggregate has reached saturated surface dry conditions.

Using a pycnometer, 500g of fine aggregate are added into the jar. Water is then added to fill approximately 90% of the remaining capacity and the pycnometer is rolled and inverted until the air bubbles dissipate. Additional water is added to the pycnometer until the level reaches the calibrated capacity and the total mass of the filled pycnometer is recorded. The aggregate is then removed from the pycnometer and oven dried. Following a 1 hour cooling period, the mass of the dried aggregate and the water-filled pycnometer is taken.

3.5.4 Compressive Strength Test (ASTM C39)

Figure 3.11 Cylinder Placed Inside Compression Machine

Compressive strength tests are done at 28 days after casting according to ASTM C39 standards using a sulfur based capping compound. Cylinders are sulfur-capped according to the standards set in ASTM C617 to ensure a flat compression surface. The capped cylinder is then loaded until breaking in a compression machine capable of applying up to 1,000,000 lb of force. Three cylinders are tested for each mix to ensure accurate and consistent results.

3.5.5 Tensile Splitting Test (ASTM C496)

Figure 3.12 Cylinder Placed in Tensile Splitting Test Machine

Tensile splitting tests are done for each mix at 28 days following ASTM C496 standards. Each specimen is placed horizontally in the testing machine between two 1-inch wide pieces of plywood. The cylinder is then loaded until splitting occurs. Three specimens are tested for each mix to ensure accuracy.

3.5.6 Modulus of Elasticity Test (ASTM C469)

Figure 3.13 Capped Cylinder with Modulus of Elasticity Rig

ASTM C469 standards are followed for the elastic modulus test. Samples are chosen and sulfur capped along with samples used for the ASTM C39 compression test. The cylinders are loaded until 40% of their compressive strength with strain readings being taken every 4,000 lb. Each cylinder is tested twice for consistency and each mix has two cylinder specimens to be tested.

3.5.7 Restrained Shrinkage Test (AASHTO PP34)

3.5.7.1 Summary of Test Method

From each mix, three AASHTO PP34 ring specimens are collected. The rings consist of a 1/2 – inch thick steel ring, outer diameter of 12 inches and a height of 6 inches, surrounded by a concrete ring measuring 3 inches in thickness and 6 inches in height. As the concrete shrinks, the steel ring is to provide sufficient restraint to induce cracking.

The molds consist of a wooden base, treated with sealant, onto which the steel ring is centered and held in place by metal screws along the inner diameter of the ring. A lined cardboard ring is placed around the steel ring ensuring an even spacing of 3 inches for the concrete to fill. Concrete is scooped into the mold and allowed to settle under its own weight. A slightly modified testing method is used for the some of the AASHTO PP34 restrained shrinkage rings based on the previous study done by Montemarano (2009). One ring for each mix has six additional strain gauges, in the shape of a hexagon, embedded into the concrete in an attempt to directly measure the strain of the concrete. A trowel is used on the ring to ensure a smooth surface and the bolts attached to the strain gauge hexagon are lowered into the wet concrete. Steel rods are laid atop the ring to keep the gauges out of the concrete. After ensuring the bolts are completely embedded into the concrete, the excess concrete is cleaned and the rings taken to storage.

After a one day wet-cure period, the wet burlap is removed and a coat of paraffin wax is poured along the top surface of the rings. When the coating dries, the cardboard tubing is removed and the rings are placed on a plexiglass surface. A lining of silicone caulk is spread along the bottom surface of the ring to ensure evaporation only occurs

from the side surfaces and the strain gauges are wired to a datalogger. Strain readings are collected at two minute intervals and readings are monitored for any indication of cracking. If cracking is suspected, the surface of the ring is observed using a digital microscope with up to 200x magnification and cracks are measured and tracked until the ring is 56-days in age.

3.5.7.2 Sensors and Instrumentation

Two kinds of strain gauges are used for the restrained shrinkage test. Along the inside of each ring are 4 evenly spaced foil strain gauges running along the circumference. Sensor wires are soldered to the contacts on the strain gauges to provide a current. The gauges are glued to the steel and sealed by a layer of epoxy to prevent moisture from damaging the gauge. The gauges, manufactured by Vishay Micro-Measurements, measure strain using a Wheatstone bridge circuit. In a Wheatstone bridge, a charge is run through the circuit and the resistance is measured. As the gauge lengthens or shortens, the circuit itself changes as well, and the resistance is altered. The change in resistance is easily converted to a strain value using a gauge factor provided by the manufacturer. To ensure proper functionality, the surface of the ring must be smoothed and cleaned prior to gauge installation and the temperature in the room must be controlled. The foil strain gauge used for this study is shown in Figure 3.14 with circuitry visible.

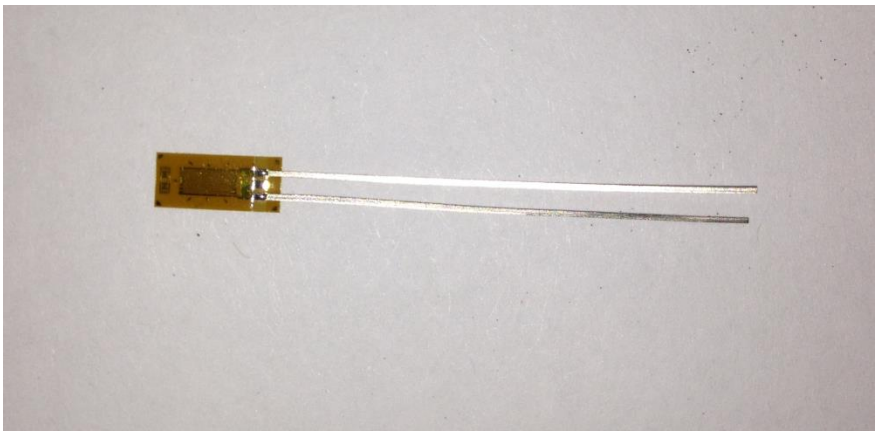

Figure 3.14 120 Ohm Foil Strain Gauge

One ring from each mix also contained six embedded vibrating wire strain gauges (VWSGs) in the shape of a hexagon. This testing method has been previously used by Montemarano (2010) in an effort to directly observe the strain and deformation occurring within the concrete. The VWSG sensors, pictured in Figure 3.15 are manufactured by Geokon Inc and work using an incased steel wire anchored tightly at two ends. As the sensor is compressed or extended, the frequency at which this wire vibrates is altered. The frequency is read using a separate device known as a plucking coil. The plucking coil is attached to a sensor wire that is attached to the datalogger system. Using the gauge factor provided, the change in frequency can be converted to a strain value. The sensors are attached using small screws to mounting brackets on each end. These mounting brackets are bolted together to form a hexagon which is embedded into the concrete. The finished hexagonal VWSG setup is shown in Figure 3.16 prior to being embedded.

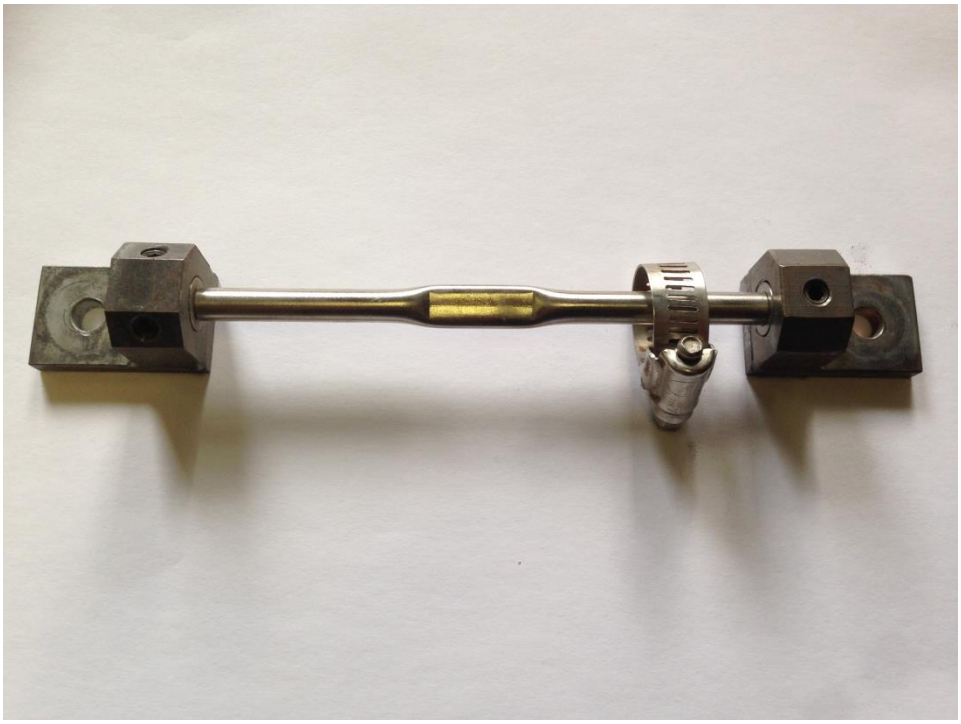

Figure 3.15 Geokon Model 4000 Vibrating Wire Strain Gauge

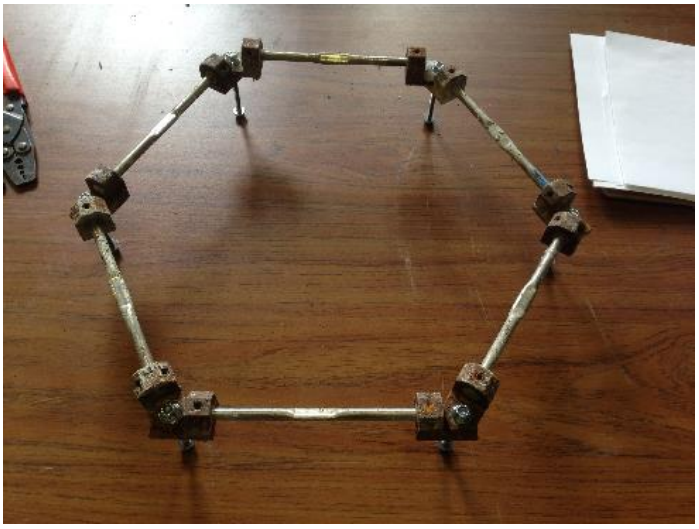

Figure 3.16 Vibrating Wire Strain Gauge (VWSG) Hexagon Setup

3.5.7.3 Sealing & Storage

AASHTO PP34 standards require the restrained shrinkage ring be sealed along the top and bottom to prevent evaporation from those surfaces. With evaporation only on the side surfaces, shrinkage will be more unidirectional and larger cracks should appear. For the top surface, blocks of paraffin wax are melted using a hot plate. The melted wax is poured directly atop the ring, still in its cardboard mold, until the entire top surface is covered. After the wax has dried, the wax is cleaned from the side and the cardboard mold can be removed. The bottom surface is sealed with a lining of silicone caulk spread across the bottom edge. The plexiglass base, combined with the silicone caulk, prevents evaporation along the bottom surface.

Ring samples are stored in an environmentally controlled chamber at a temperature of 74 degrees Fahrenheit and 50% relative humidity. For the first 24 hours, the samples are covered in layers of wet burlap with water at 74 degrees Fahrenheit. After a 24 hour wet cure, burlap is removed and the samples are stored on shelves and sensors are wired to a datalogger for the duration of the testing. The finished ring specimen are shown in Figure 3.17 with sensors and in Figure 3.18 without sensors.

Figure 3.17 Finished Restrained Shrinkage Ring with Embedded Sensors

Figure 3.18 Finished Restrained Shrinkage Ring without Embedded Sensors

3.5.7.4 Data Collection & Analysis

Each mix consists has 12 Foil Strain Gauges (FSGs) and 6 VWSGs. With up to four mixes being tested simultaneously, a total of 72 data channels need to be logged. With collection intervals of two minutes over the course of 56 days, over 2.9 million data entries will be collected. For this reason, a data logging system is required to automate the process. A modular system manufactured by Campbell Scientific is used. The system allows us to collect data from both types of sensors at two minutes intervals, converting the raw data into strain values and stores the data on a hard drive for collection and processing.

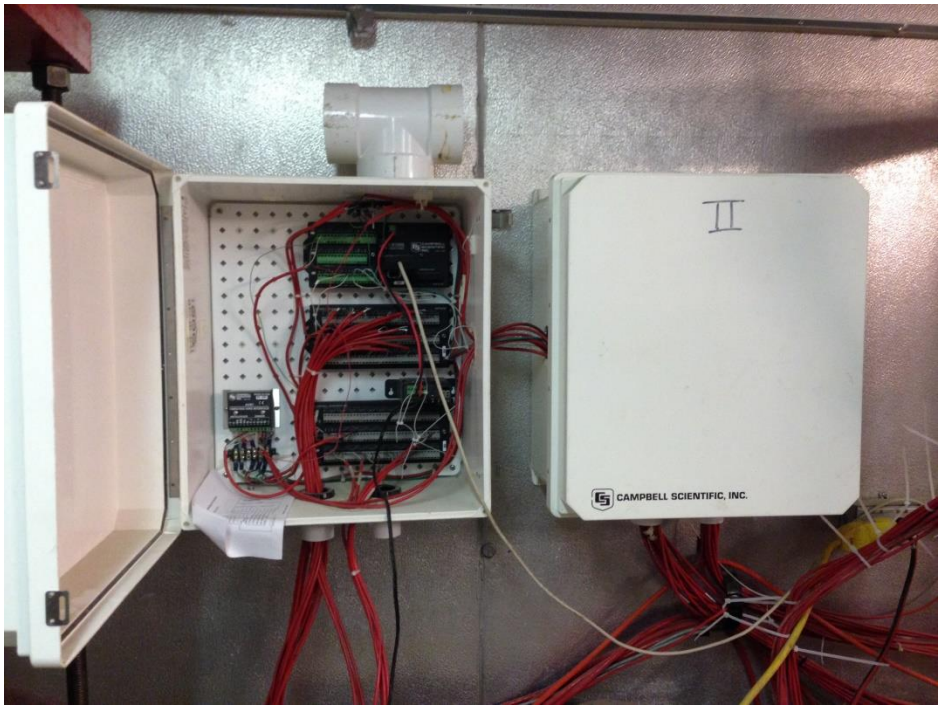

Figure 3.19 Data Logging Unit from Campbell Scientific

The data logging unit used for this experiment is shown in Figure 3.19. Data is collected every 2 to 3 days; temperature and humidity readings are checked and strain

readings are checked for any indication of cracking. Vibrating wire or foil strain gauges that exceed the cracking strain threshold, defined by the concrete's tensile strength divided by the elastic modulus, are indicative of a crack forming. The equation is shown in Equation 3.7 where ε is the cracking strain, σ is the ultimate tensile strength and E is the modulus of elasticity.

$$\varepsilon_t = \sigma_t/\mathrm{E} \tag{3.7}$$

3.5.8 Free Shrinkage (ASTM C157)

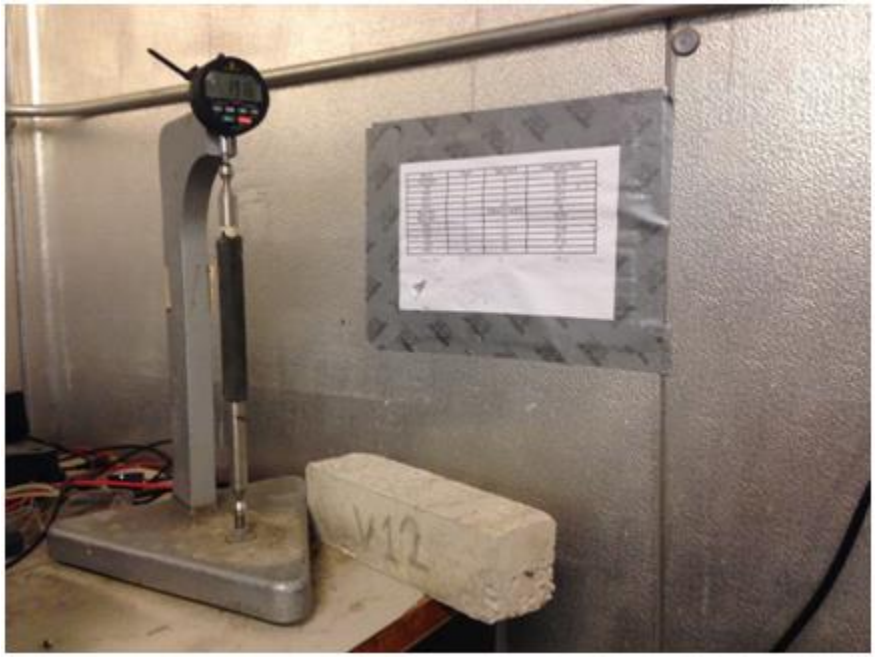

Figure 3.20 Length Comparator and Prism Sample

Free shrinkage measurements are taken regularly using a length comparator and prisms measuring 3 x 3 x 10 inches. With each mix, two prism samples are cast with embedded studs at either end. Samples are stored and tested in an environmentally

controlled environment to prevent any thermal expansion. At each testing period, a reference bar is placed into the length comparator and the length reading is taken. The prism sample is then placed into the length comparator and the measurement is recorded. The process is repeated for each sample of each mix at every testing period. Samples are tested at least once weekly over the 56-day testing period.

CHAPTER IV

4 RESULTS

4.1 INTRODUCTION

The results for all concrete testing are summarized in the following chapter. The testing includes wet concrete properties of workability, flowability, unit weight and air as well as hardened concrete properties of strength, elastic modulus and shrinkage. The specific tests performed and their respective procedures are summarized in Section 3.5. The wet concrete results will be covered first, describing the necessary adjustments made while the mix was still in its plastic state, followed by the strength and elastic modulus results and last, the free and restrained shrinkage results will be presented.

4.2 FRESH CONCRETE TEST RESULTS

4.2.1 Slump Flow

The slump flow test is done according to the procedure described in ASTM C1611 using an inverted slump cone. Slump flow is the first test performed after the concrete mix is prepared. Because the mixes are self-consolidating, a high slump flow is necessary to facilitate in pouring. For this set of mixes, the given slump range is 21.5 inches (550 mm) to 25.5 mm (650mm). After the control mix, PPE 0.00, achieves the

required slump value, each subsequent mix is first tested using the same dosage of water-reducer. To offset the reduction of slump flow due to the addition of fibers, water-reducer is added resulting in the "Adjusted Slump" value. Figure 4.1 shows the slump values of the adjusted and non-adjusted mixes.

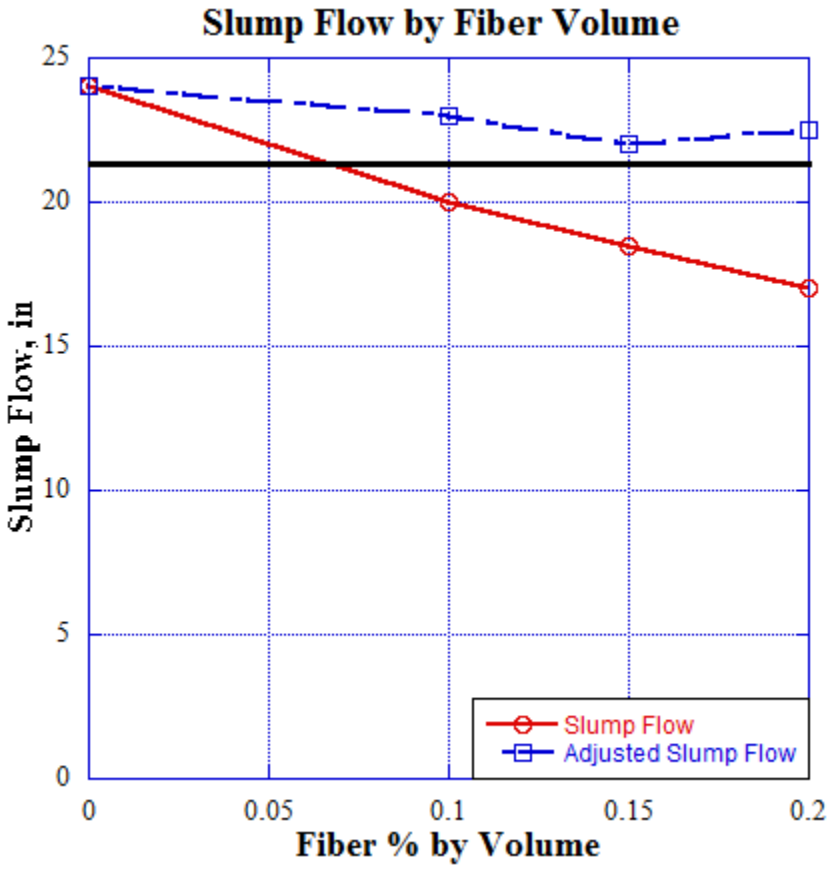

Figure 4.1 Slump Flow & Adjusted Slump Flow of FRSCC Mixes

As expected, without the water-reducer additions, the mixes fall below the minimum required slump flow, as indicated by the horizontal line on the graph, with as little as 0.10% fiber by volume. With adjustments, however, the minimum slump flow

can be achieved with fiber additions exceeding 0.20% by volume. The slump values are tabulated in Table 4.1.

Table 4.1 Original and Adjusted Slump Values

Slump Results	PPE 0.00	PPE 0.10	PPE 0.15	PPE 0.20
Slump Flow, in	24	20	18.5	17.5
Adjusted Slump, in	24	23	22	22.5

When comparing the slump losses to those found in El Dieb and Taha's (2011) study, a similar pattern is noticed. Because our control mix starts at a lower slump of 24 inches as opposed to the study's 27.5 inches, the initial loss from the addition of fibers is somewhat larger. A loss of approximately 17% is observed when fibers are added at 0.10% by volume, compared to an 11% in El-Dieb and Taha's study. When an additional 0.05% of fiber volume is added to the mix, an additional 8% of slump loss is observed, equal to the loss observed by El-Dieb and Taha. When fiber volume is increased again to 0.20%, another 5% of slump loss is observed, similar to the 6% observed by El-Dieb and Taha (2011).

Table 4.2 summarizes the amount of high range water-reducer added to each of the mixes. The additional water added as a result of these mixes is accounted for in the given water to cement ratio tolerances.

Table 4.2 Water Reducer Additions for FRSCC Mixes

Mix Adjustments	PPE 0.00	PPE 0.10	PPE 0.15	PPE 0.20
High-Range Water Reducer, fl oz/cu yd	68	81	81	95
Fiber % by volume	0	0.1	0.15	0.2

4.2.2 T20

The T20 test occurs during the slump test. The elapsed time, in seconds, between lifting the slump cone and the slump flow exceeding 20 inches in diameter is measured. To ensure the mix is stable and that self-consolidation will happen within a relatively short period of time, the T20 time should exceed 2s but not exceed 20s. A low-viscosity SCC mix is generally preferred and for this, a T20 time of close to 5s is desired. The T20 test results are summarized in Table 4.3.

Table 4.3 T20 Test Results

T20	PPE 0.00	PPE 0.10	PPE 0.15	PPE 0.20
T20, s	6.1	5.5	7	9.6

The viscosity is markedly increased towards the higher end of the fiber addition rates. While the total slump remained relatively close for each mix, the flow did move slower for the higher fiber mixes.

4.2.3 Visual Stability Index (VSI)

The Visual Stability Index (VSI) is taken immediately after the slump flow measurements are taken. The VSI for the four mixes tested in this study are summarized in Table 4.4.

Table 4.4 Visual Stability Indices

VSI	PPE 0.00	PPE 0.10	PPE 0.15	PPE 0.20
VSI	0	0	1	1

The first two mixes show a homogenous slump flow indicating a VSI of 0, this mix is unlikely to segregate or bleed even when mixed in higher volumes. As fibers are added and slump flow is inhibited slightly, a halo-like ring is formed around the slump flow consisting of water and cement. This ring is the first indicator that segregation may occur. For PPE 0.15 and PPE 0.20 the ring remained small and the aggregate did not visibly segregate, indicating a VSI of 1. While a VSI of 1 is the highest found in the mixes in this study, trial mixes have shown that additional fibers could lead to a higher degree of segregation. A VSI of 0 is considered ideal; however a VSI of 1 is acceptable in most cases. A VSI of 2 or 3 indicate the mix is not ready for real-world application and additional measures must be taken to reduce segregation.

4.2.4 J-Ring

The J-ring test is done after the slump, T20 and VSI is taken. Determining the passing ability of an SCC mix is important for construction applications in which the concrete must pass through tightly spaced reinforcement bars. As the J-ring value is highly dependent on the slump of the concrete, a mix is considered to have an adequate passing ability if the J-ring is within three inches of the slump. The J-ring values are displayed in Table 4.5.

Table 4.5 J-Ring Test Results

Mix	**PPE 0.00**	**PPE 0.10**	**PPE 0.15**	**PPE 0.20**
J-ring, in	22.5	21	19	17
+/- Slump	-1.5	-2	-3	-5.5

We see that mixes containing fibers up to 0.15% by volume can pass the J-ring specifications given. However, once fibers are increased further, passing ability becomes a concern; with mix PPE 0.20 showing a flow loss of 5.5 inches in the presence of tightly packed reinforcement. The use of a mix with a high fiber content, specifically PPE 0.20, is not advised in when reinforcement spacing is small, however PPE 0.20 may still have some real-world application, especially in situations where slight consolidation is possible.

4.2.5 L-Box

Though it is not a standardized test, the L-box test can be used to identify a mix with potential passing ability problems. The L-box setup used in this study uses closely spaced reinforcement as described in section 3.4.4. Though no value is specified, for this study, a desirable h1/h2 ratio for an SCC mix will be below 2.0. For L-box values above 2.0, the SCC will have trouble passing through reinforcement in confined spaces such as the inside of parapets or the flanges of concrete beams. The L-box results are shown in Table 4.6.

Table 4.6 L-Box Values for FRSCC

Mix	PPE 0.00	PPE 0.10	PPE 0.15	PPE 0.20
L box	1.2	1.5	2	2.5

Similar to the J-ring test, we notice mix PPE 0.20 did not pass the specified L-box measurements. As a result of these two tests, we can see that the addition of fibers at

0.20% by volume may cause consolidation problems in confined or heavily reinforced spaces.

4.2.6 Air Tests

Two air tests are conducted in this study for redundancy. Adequate air entrainment will allow for pouring in regions where concrete is subjected to freeze and thaw cycles. For these mixes, the targeted air content is between 4 – 8% by volume. The results of the two air content tests are displayed in Table 4.7.

Table 4.7 Air Content for FRSCC

Mix	PPE 0.00	PPE 0.10	PPE 0.15	PPE 0.20
Air Content (Pressure)	7	7	7.8	8
Air Content (Gravity)	6.2	6.5	7.1	6.9

The air content differs slightly between tests, however the variance is sufficiently small and both values are within the desired air content range. As fiber is added, air content rises slightly, however this is likely a side-effect of the increased high-range water reducer used in the high fiber mixes. Concrete performance in freeze and thaw cycles is not expected to suffer.

4.3 MECHANICAL PROPERTIES

Mechanical properties are tested for the FRSCC mixes at 28 days after mixing. In between casting and testing, the samples are stored in the environmental chamber to provide steady ambient conditions, identical to those for the shrinkage samples. When the

samples are ready to be tested, they are removed from the environmental chamber and, if applicable, capped and tested.

Nine samples from each mix are used for the testing. Six samples are capped using a sulfur capping compound, three of which are compressed while three are used for elastic modulus testing. The final three samples are used for the tensile splitting test. The results for the testing are summarized in Table 4.8.

Table 4.8 Mechanical Properties

	PPE 0.00	**PPE 0.10**	**PPE 0.15**	**PPE 0.20**
Compressive Strength, psi	5,632	5,364	5,494	5,130
Tensile Strength, psi	361	385	398	410
Elastic Modulus, ksi	4,295	4,165	4,210	3,981
Cracking Strain, ue	84	92	95	103

Also included in Table 4.8 is the cracking strain value for each mix. The cracking strain is the expected strain a mix could sustain before cracking begins; a value important for the restrained shrinkage testing. Equation 4.1 shows how the cracking strain value is obtained.

$$\text{Cracking Strain } (\mu\varepsilon) = \frac{\text{Tensile Strength}}{\text{Elastic Modulus}} \tag{4.1}$$

We notice that, as fiber content is increased, compressive strength slightly decreases. This is because the strength of the concrete comes from the bond between cement and aggregate; the flexible fibers mixed into the cement matrix are not stiff enough to significantly improve compressive strength. Between 0.00 and 0.20% fiber by volume, compressive strength drops approximately 9%. Elastic Modulus also decreases

by a small margin of approximately 7%. Statistically, these values are very small because of the relatively small fiber range used in this experiment. The tensile splitting strength, however, shows a slightly more significant change. When fiber volume is increased to 0.20% the tensile strength increases by almost 14%. Tensile strength increases because of the fiber's tendency to provide resistance to pull-out forces, caused by friction between the cement matrix and the fiber themselves. The increase in tensile strength is a major contributor to the increase in cracking strain and is key to decreasing cracking in restrained shrinkage.

4.4 FREE SHRINKAGE

Comparator measurements for free shrinkage are taken throughout the testing period at least twice every week. The free shrinkage of each mix is an indicator of the stresses we expect to see in the restrained shrinkage rings. The free shrinkage results are shown in Figure 4.2.

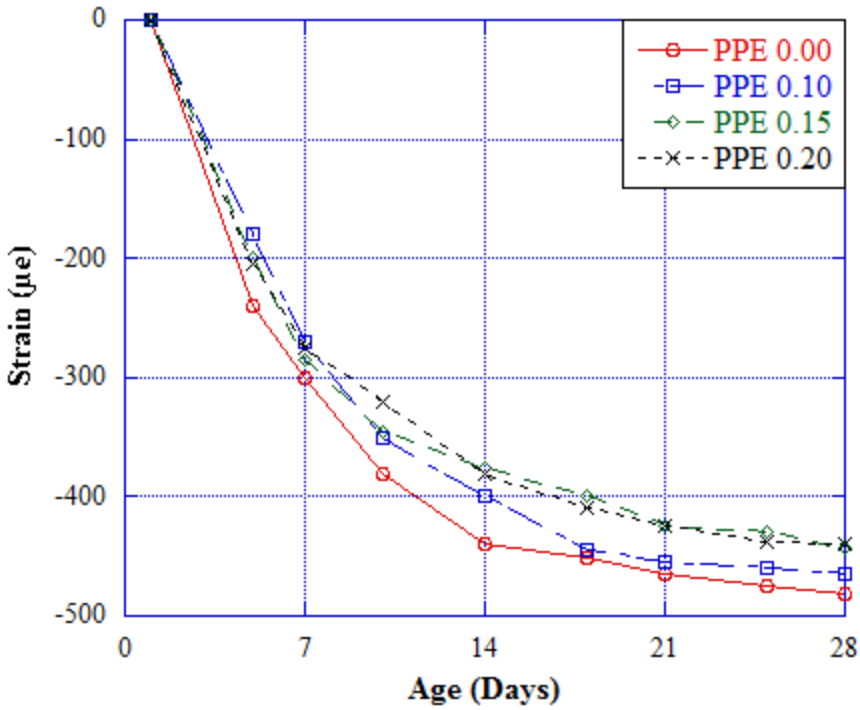

Figure 4.2 Free Shrinkage Strain

We notice a decrease in free shrinkage as fiber content increases. When polypropylene fibers are added at 0.20%, free shrinkage decreases by approximately 9%. While relatively small, this decreasing trend is expected to continue as fibers are increased; Saje et al. found that free shrinkage decreases until fiber volume exceeds 0.75% (2011). As a result, we can expect strains in the restrained shrinkage specimen to be lower in FRSCC mixes and, given the cracking strain results from the previous section, cracking will require a higher overall stress as well. As a result of these two factors, less cracking is expected in a restrained shrinkage case.

4.5 RESTRAINED SHRINKAGE

4.5.1 Method of Analysis

The restrained shrinkage testing is done with the use of AASHTO restrained shrinkage rings. A ½ inch thick, 12-inch outer diameter, 6 inch tall steel ring is surrounded by 3 inches of concrete. Once cast, the sample is cured for 24 hours under wet burlap. The burlap is then removed and the samples are allowed to sit in the environmental chamber for the remainder of the testing period.

Two samples are cast for each mix, the first with strain gauges attached to the inner surface of the steel ring and six embedded strain gauges forming a hexagon along the top surface of the ring. The second ring sample contains only the steel strain gauges. Each sensor is monitored regularly for any indications of cracking on the ring. Once a crack is found, a digital microscope is used to observe the crack over the remainder of the testing period and check for propagation as shrinkage continues.

AASHTO standards, as well as numerous studies, typically only use steel strain gauges as a means of calculating concrete strain. The strain values from evenly distributed points along the ring are averaged, with the assumption that strain in the concrete is evenly distributed. This study compares the strain obtained from the traditional steel strain method to those obtained from partially embedded vibrating wire strain gauges. By directly collecting strain from the concrete, the stress distribution across the ring can be more accurately represented and the deformation as a result of the shrinkage can be modeled. The samples will also be observed for any inadvertent extra cracking that may be caused as a result of the embedded steel bolts.

4.5.2 Results

4.5.2.1 PPE0.00

Mix PPE0.00's restrained shrinkage results are shown in the strain graphs in Figure 4.3and Figure 4.4. The crack-maps taken over the course of crack development up to 28 days are shown in Figure 4.5.

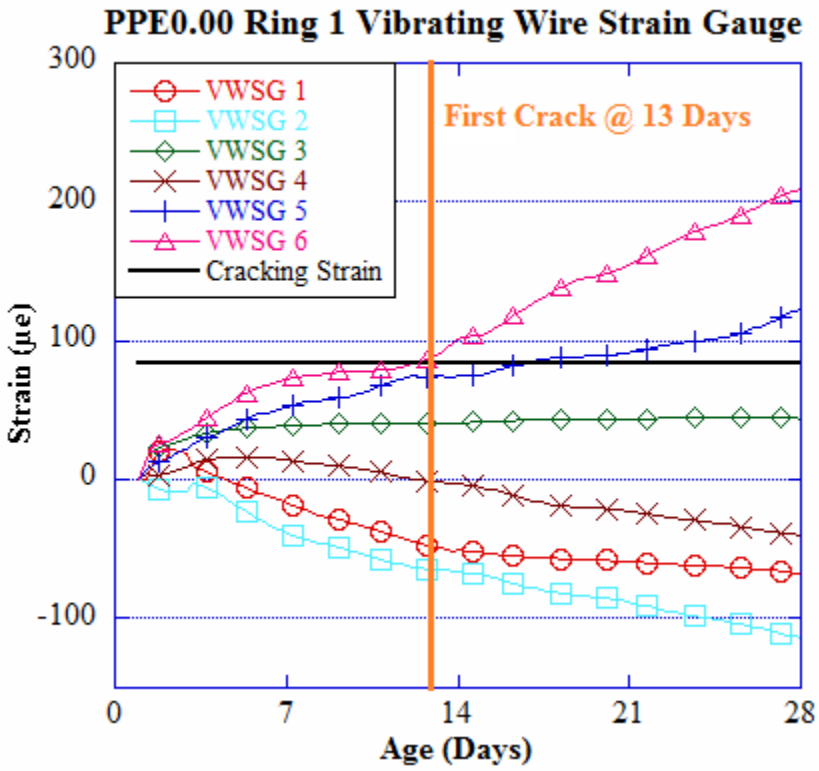

Figure 4.3 Mix PPE0.00 Ring 1 Vibrating Wire Strain Graph

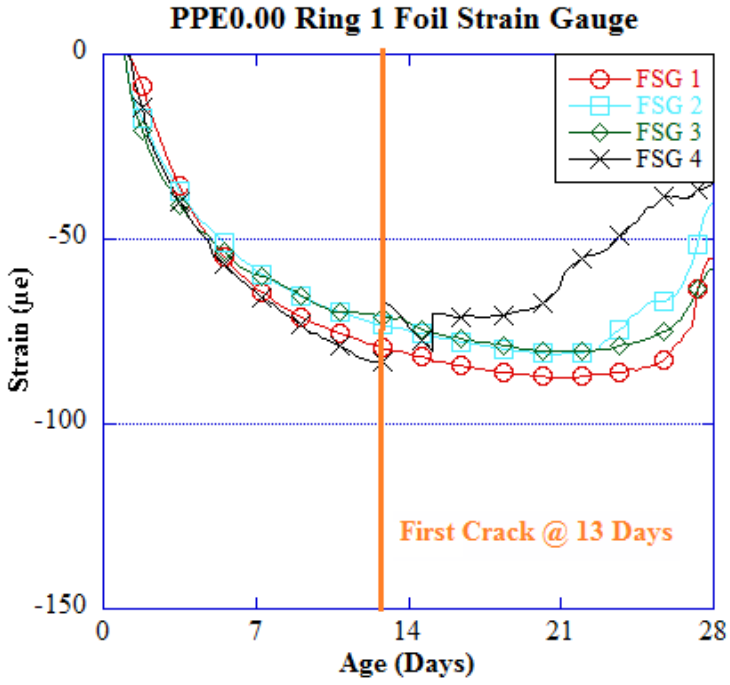

(a)

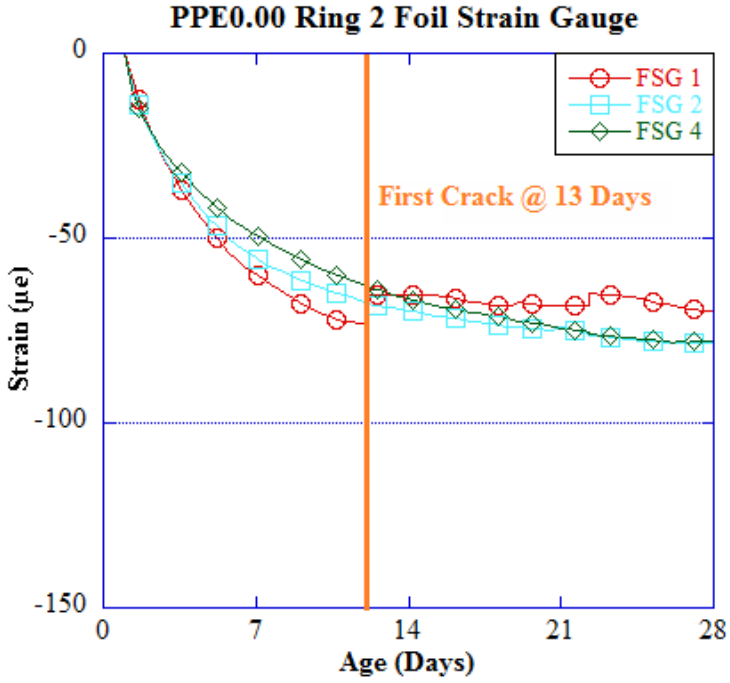

(b)

Figure 4.4 Foil Strain Gauges from (a) Ring 1 and (b) Ring 2

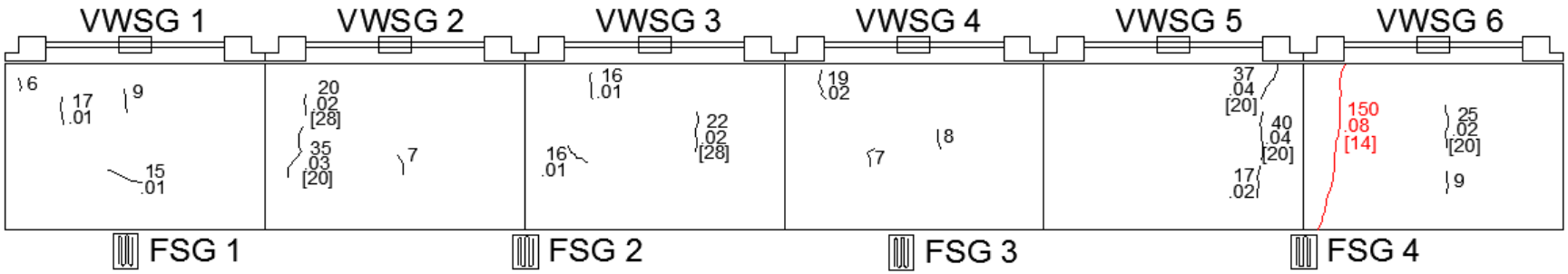

(a)

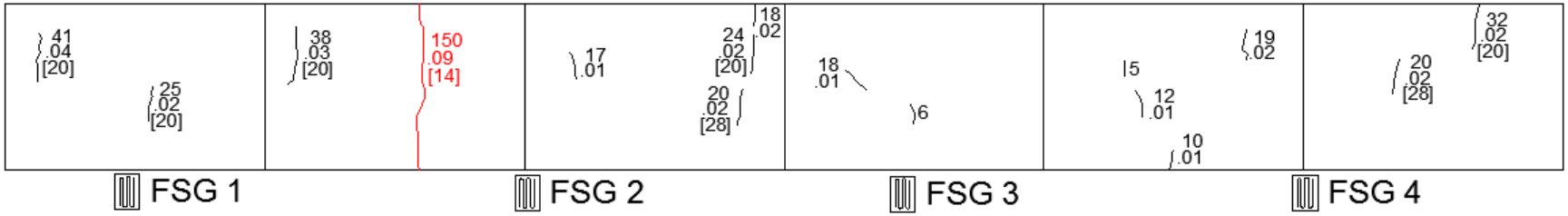

(b)

Figure 4.5 Crackmaps from mix PPE0.00 (a) Ring 1 and (b) Ring 2

The control SCC mix, PPE0.00, shows extensive cracking by the end of the testing period. Once removed from curing, stress began developing immediately, as shown by the steep curves of the foil strain gauges in Figure 4.4a. Over time, as the rate of shrinkage decreases, we see the rate of stress buildup in the steel also decreases.

In Ring 1 in particular, we see this stress lead to the formation of an initial crack at approximately 13 days. The foil strain gauges are the first to detect a change in the concrete early on the 13th day when a sizable drop in strain is detected in FSG 4. This loss of restraint indicates cracking may have begun in that quadrant of the ring. Shortly thereafter, VWSG 6 of the same ring detects a strain exceeding the expected cracking strain of this mix. VWSG 5 shows a large positive strain as well, though at 13 days of age this strain is below the cracking strain. As these sensors are directly measuring concrete strain, we examine the ring for cracks as the sensor strain value approaches the cracking strain value obtained from concrete strength tests.

The surface of the ring is checked for cracking as soon as either the FSG or VWSG indicate potential cracking. On the 13th day for the first ring, no cracks were found. A preliminary crack-map done on the 14th day began to show the formation of a crack within the region covered by VWSG 6. This indicates that cracking began along the steel on the 13th day and worked its way outward by the 14th day. However, on first observation, this crack had not propagated the full height of the ring. Days later, a full crack-map was done on the entire surface of the ring and additional cracking was found, mostly concentrated in the area covered by VWSG 5 and VWSG 6. Comparing this to the strain graphs, we see that around 19-20 days, the strain value for VWSG 5 has also exceeded the cracking threshold of 83 microstrains, and so cracking in that region is to be

expected. We notice the rate of increasing strain in VWSG 5 and 6 steadily climbs from day 14 to 28 even as cracking has already occurred. As the cracks expand, the VWSG value becomes less indicative of the conditions within the concrete and eventually, once the crack fully propagates, measures only the width of the crack.

Full propagation of the major crack in VWSG 6, shown in red in Figure 4.5a, occurs by day 20. Once the crack propagates the entire height of the ring, a slight relaxation is shown throughout all the foil strain gauge sensors and the restraint provided by the steel ring is reduced. Small, localized, cracking is still possible after the relaxation occurs due to internal stresses in the concrete, however, this cracking is insignificant in comparison to the restrained shrinkage cracking.

Ring 2, with only the foil strain gauges attached, shows a similar pattern in stress development. While one gauge malfunctioned, the remaining three show stresses increasing at a similar, if slightly slower, rate. The crack, occurring around the 13^{th} day according to the FSG sensors, happens in the region of FSG 1. By the time of cracking, the average strain in the FSG sensors of Ring 2 are just above 10% lower than those of Ring 1. While, alone, this is inconclusive, it could be indicative of a trend in the VWSG rings.

The crack-maps for Ring 2 show a similar pattern to Ring 1. The crack, initially observed at 14 days, formed in the area between FSG 1 and FSG 2. Smaller cracks later formed in other regions of the ring, however these did not amount to any significant crack. By 20 days, the major crack, shown in red in Figure 4.5b, had extended the entire height of the ring. Through the wax, a small opaque line is visible which indicates the

hardened paraffin wax has split due to the pulling apart of the crack. The faint line is visible in Figure 4.6.

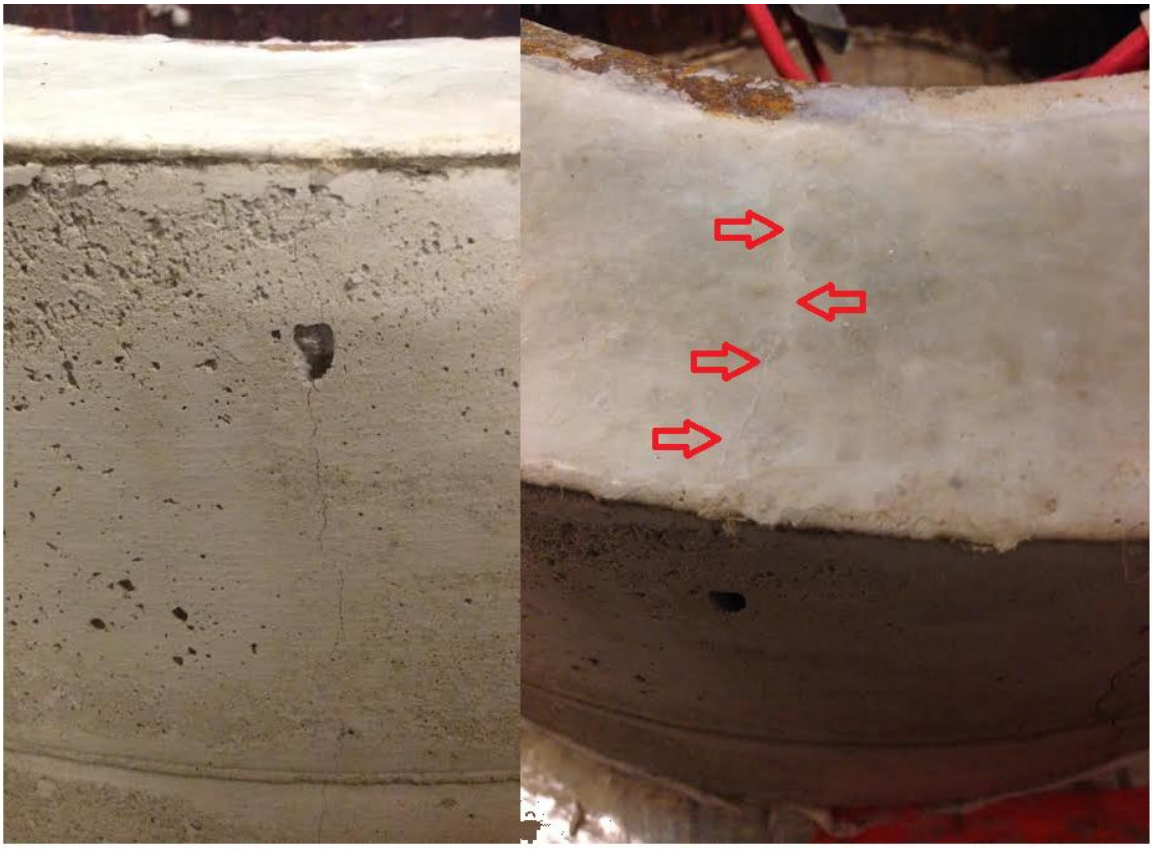

Figure 4.6 Crack visible in Ring 2 from the Side and Above

Mix PPE0.10's restrained shrinkage results are shown in the strain graphs in Figure 4.7, Figure 4.8, and Figure 4.9. The crack-maps taken over the course of crack development up to 28 days are shown in Figure 4.10. The numbers next to each crack indicate, in order, the height in millimeters, the width in millimeters and the day they were first observed.

4.5.2.2 PPE0.10

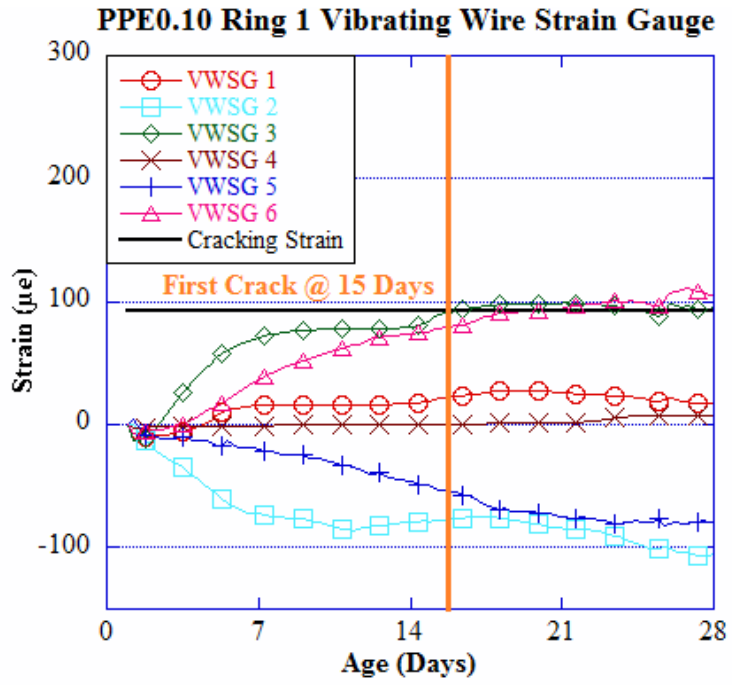

Figure 4.7 PPE0.10 Ring 1 Vibrating Wire Strain Gauge Graph

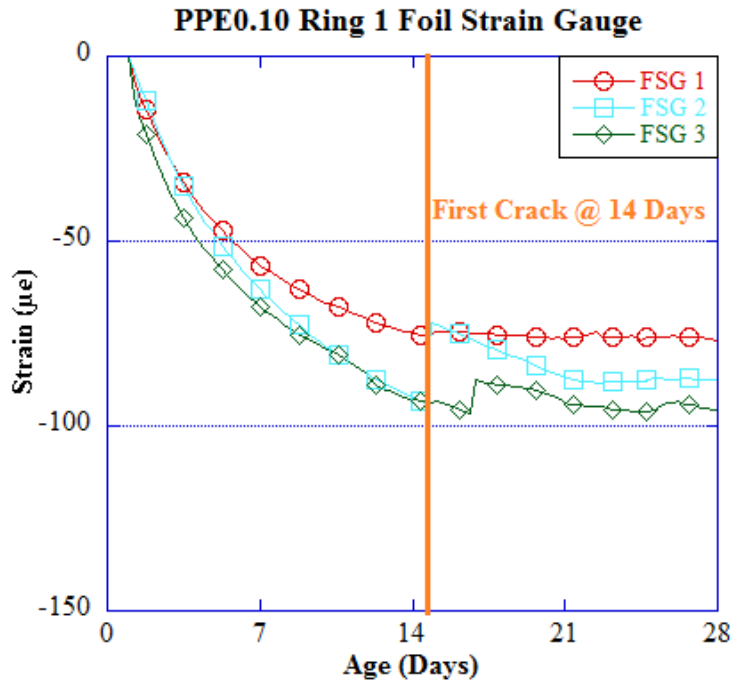

Figure 4.8 PPE 0.10 Ring 1 Foil Strain Gauge Graph

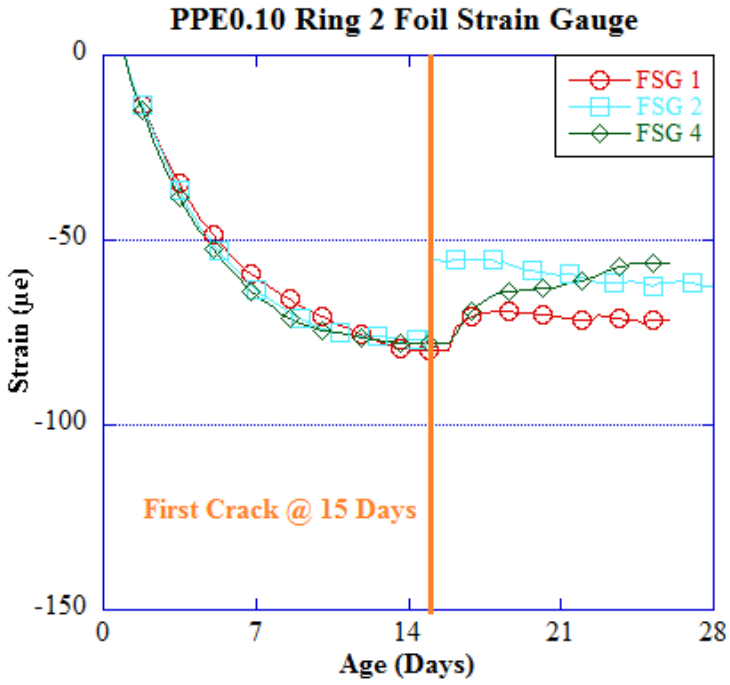

Figure 4.9 PPE 0.10 Ring 2 Foil Strain Gauge Graph

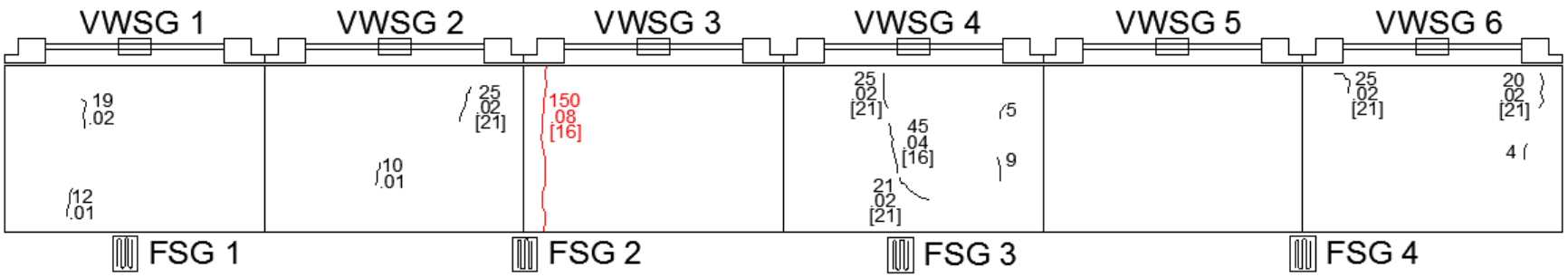

(a)

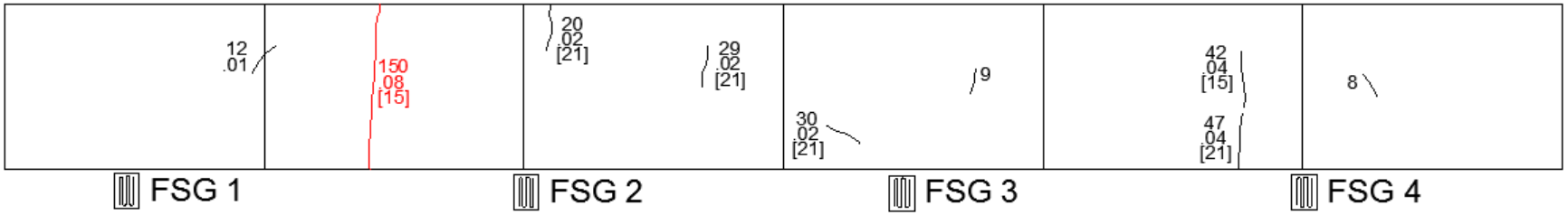

(b)

Figure 4.10 Mix PPE 0.10 Crack-maps for (a) Ring 1 and (b) Ring 2

The addition of 0.10% polypropylene fibers has a small, but noticeable, affect on the shrinkage of the concrete. Free shrinkage is slightly reduced at 28 days, falling by approximately 4%, while the cracking strain is increased by almost 6%. Combined, these two factors should lead to less shrinkage induced cracking.

Ring 1 of Mix PPE0.10 showed tensile stresses concentrated at opposite ends of the ring near VWSG 3 and VWSG 6 as shown in Figure 4.7. The foil strain gauges indicate a crack should have formed at 14 days, however initial crack-maps did not show any cracks along the surface. The cracks appeared on the surface two days later, on day 16, under VWSG 3, in the quadrant of FSG 2. Smaller cracking was noticed near FSG 3. By day 17, VWSG 3 had exceeded the cracking strain of 92 microstrains, indicating that cracking had occurred at the depth of the strain gauges.

As time passed, these cracks were monitored regularly. By 21 days, it became apparent that the cracking around VWSG 3, shown in red in Figure 4.10a, had propagated the full height of the ring, while the growth in the cracks under VWSG 4 had slowed. Once the crack has fully propagated, we see the strain in the steel level off indicating no significant stresses are building in the ring and no new shrinkage cracks are forming.

Ring 2 of mix PPE 0.10 follows a similar pattern to Ring 1 through the first 14 days. Figure 4.9 shows at 14 days, FSG 2 jumps significantly, indicating a likely crack in that region. A crack was found the next day, day 15 between FSG 1 and FSG 2 that was likely the source of the jump. The crack, shown in red in Figure 4.10b, eventually extended the entire height of the ring. Shortly after the first jump, approximately at 17 days, the remaining two working sensors also experienced a sudden loss in strain. This loss of strain was likely caused by additional cracks forming in the region around FSG 4

as well as the growth of the main crack around FSG 2. By 20 days, the crack became visible through the layer of paraffin wax coating the top surface of the ring and stresses in all sensors leveled off or fell indicating a loss in restraint along the ring.

Both rings of mix PPE 0.10 follow the pattern observed in previous studies in which cracking first starts along the interface between steel and concrete and propagates outward towards the surface (Hossain & Weiss, 2006).

4.5.2.3 PPE0.15

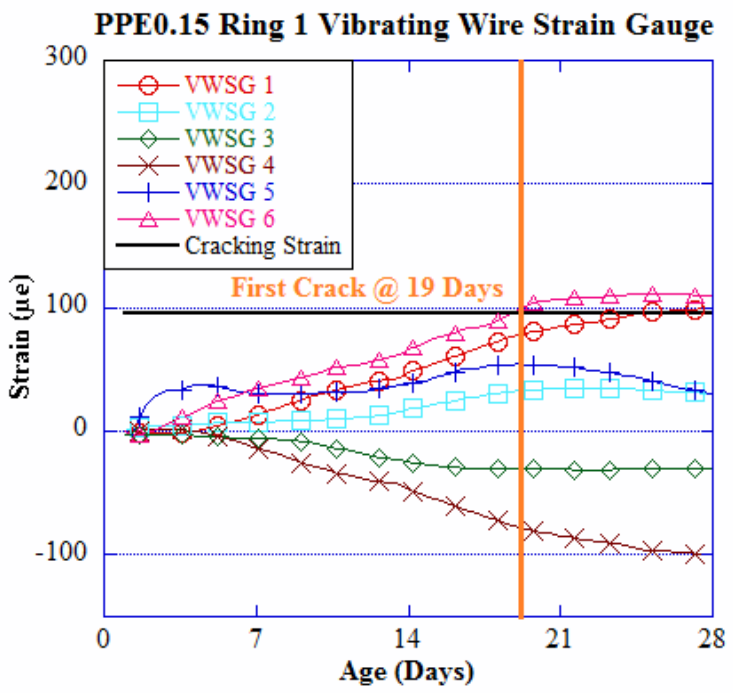

Figure 4.11 PPE0.15 Ring 1 Vibrating Wire Strain Gauge Graph

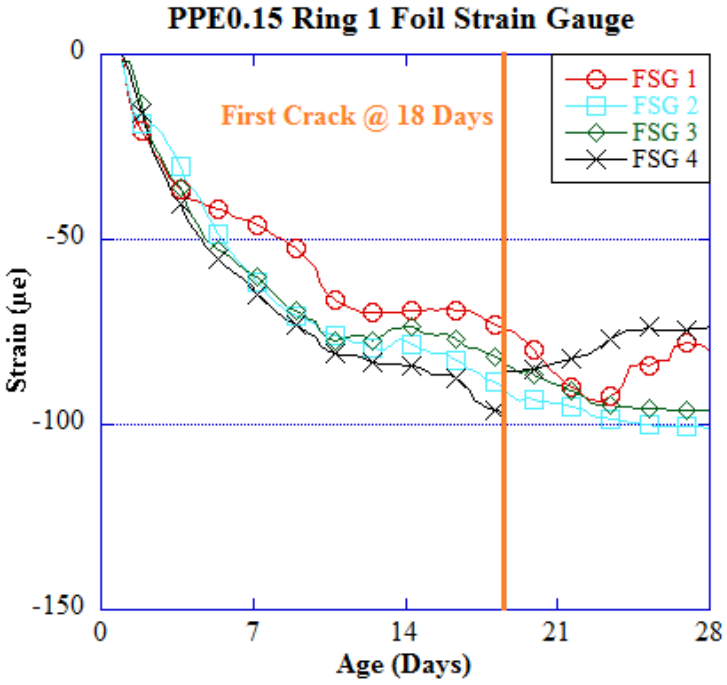

Figure 4.12 PPE0.15 Ring 1 Foil Strain Gauge Graph

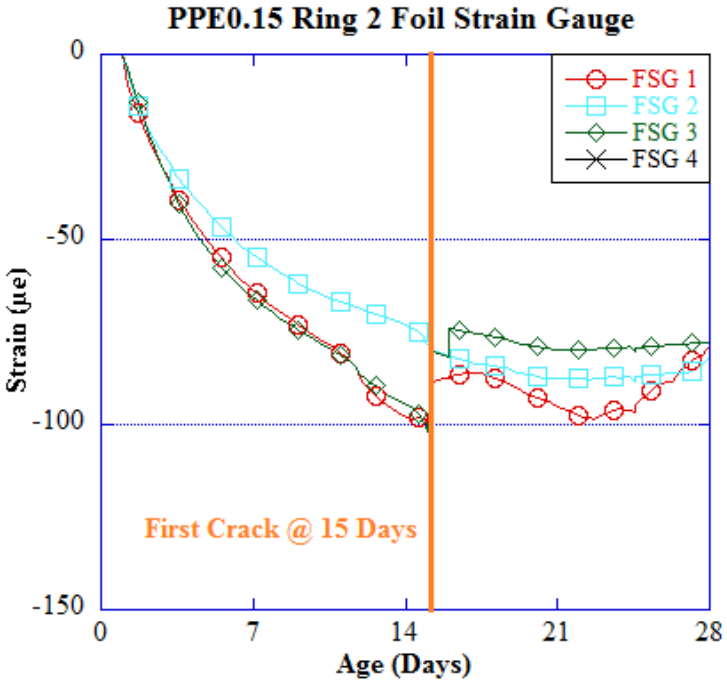

Figure 4.13 PPE0.15 Ring 2 Foil Strain Gauge Graph

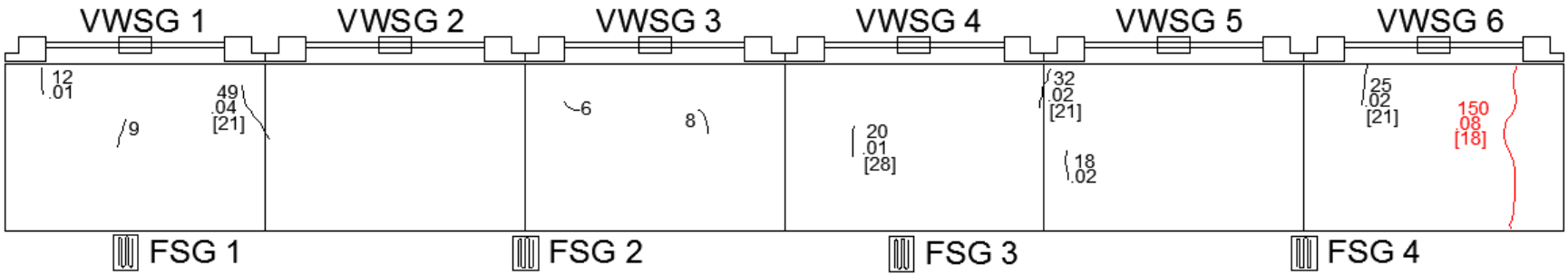

(a)

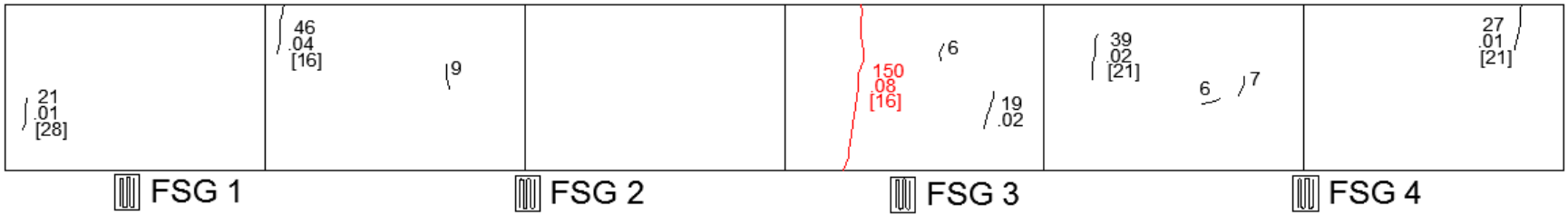

(b)

Figure 4.14 Mix PPE 0.15 Crack-maps for (a) Ring 1 and (b) Ring 2

With 0.15% polypropylene fibers added by volume, the workability and passing ability of the concrete decreased noticeably. However, the benefits the additional fibers had towards shrinkage and strength were significant. Because of the increased tensile strength, tensile cracking strain increased by 14% compared to the base SCC mix. Additionally, free shrinkage decreased by 9% in relation to the control.

Restrained shrinkage stresses in Ring 1 developed more slowly than in previous mixes. Foil strain gauges indicate the first crack to happen at around 18 days centered on FSG 4, later than the control and mix PPE0.10. The crack was observed during the crack-map done later on the 18th day as shown in Figure 4.14a in red. The VWSGs, shown in Figure 4.11, did not exceed the cracking strain threshold until shortly after 19 days, unlike previous mixes where the VWSG indicated cracking just before the crack was visible. Once VWSG 6 indicated a possible crack, strains in nearby sensors decreased, notably in VWSG 5.

After initial cracking, strain in the steel continued to build in the other three FSG sensors. Secondary cracking may have occurred around 22 days when the compressive strain in FSG 1 begins to decrease. Small cracks were observed in the region of FSG 1 the day prior to the indication of cracking; these cracks grew by 28 days to the sizes represented in Figure 4.14a.

As with the other mixes, the cracking in Ring 1 propagated outward and increased lengthwise as time went on. By 23 days, just after the second VWSG (VWSG 1) had shown signs of cracking, the first crack propagated to the steel and the wax had visibly separated on the top surface and, as seen in both the VWSG and FSG graphs, strain values leveled off.

The second specimen of mix PPE 0.15 was found to have cracking earlier than Ring 1 despite the presence of embedded strain gauges which could have caused weak points within Ring 1. Two of the FSG sensors attached to the ring simultaneously jumped at approximately 15 days. When the surface was examined, no cracks were found until the 16th day, when two cracks were found, a large one, shown in red at 28 days in Figure 4.14b, and another crack between FSG 1 and 2. Strain continued to increase in the three FSG sensors after the first cracks formed until approximately 21 days. A crackmap done at 22 days found that the initial cracking near FSG 3 had reached the full height of the ring, thus explaining the relaxation of the steel. While cracking in the second ring started earlier, it was not as extensive as in Ring 1.

4.5.2.4 PPE0.20

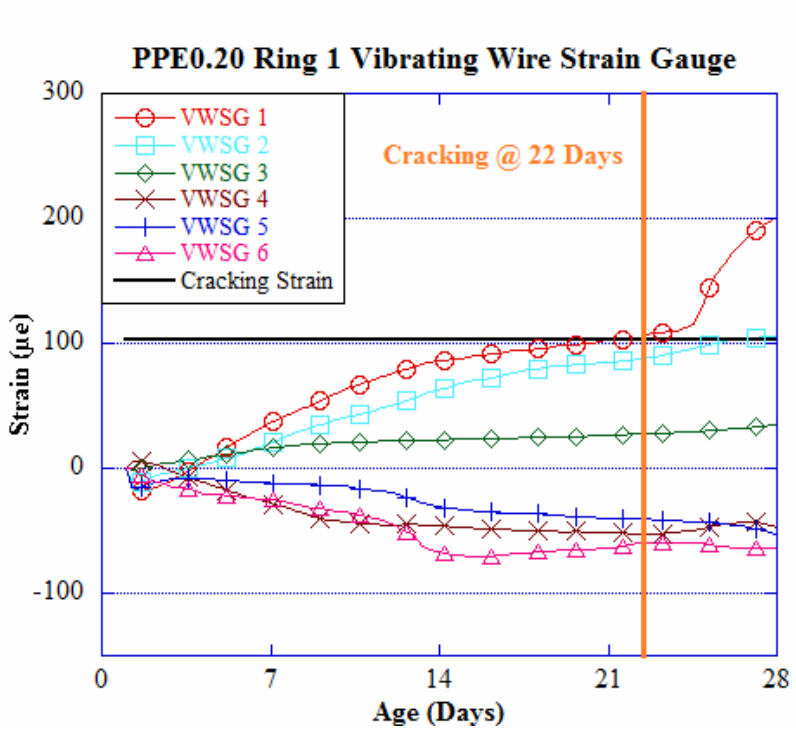

Figure 4.15 Ring 1 Vibrating Wire Strain Gauge Graph

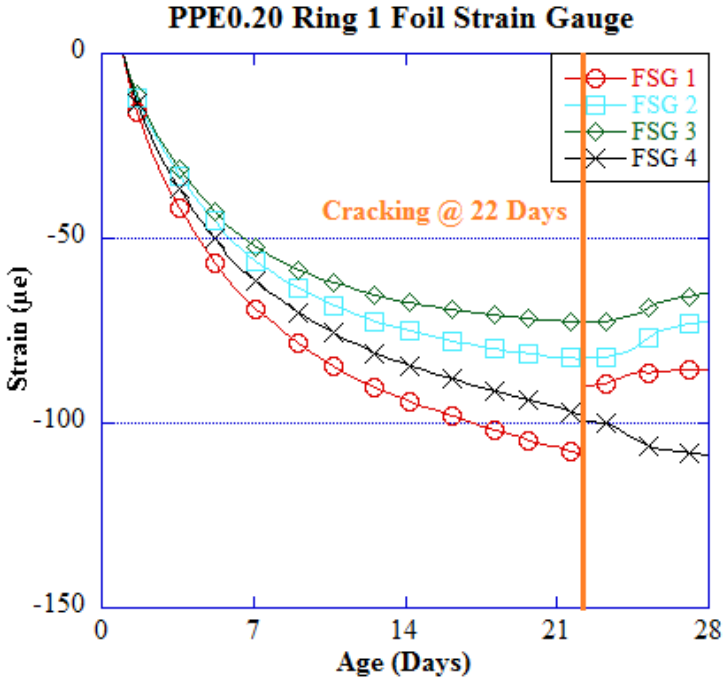

Figure 4.16 PPE 0.20 Ring 1 Foil Strain Gauge Graph

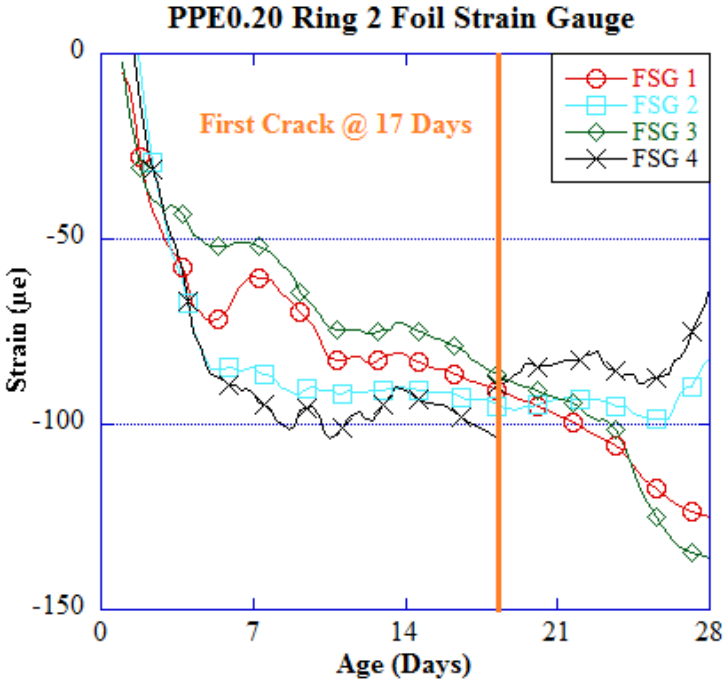

Figure 4.17 PPE0.20 Ring 2 Foil Strain Gauge Graph

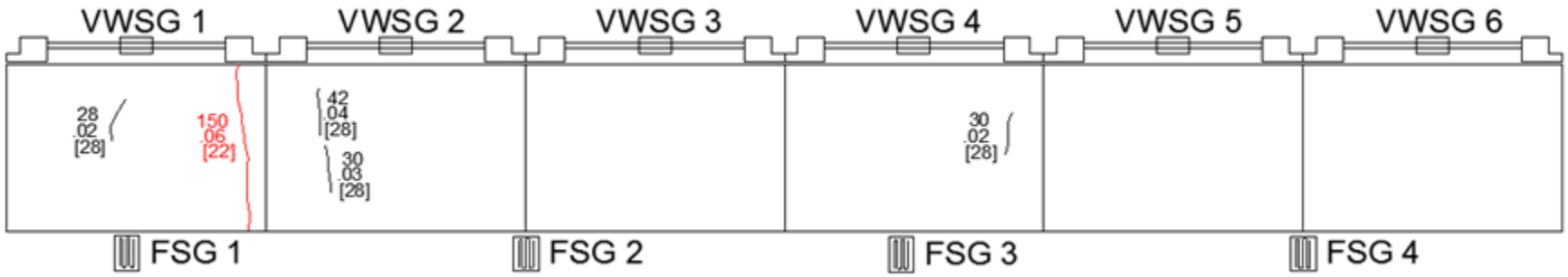

(a)

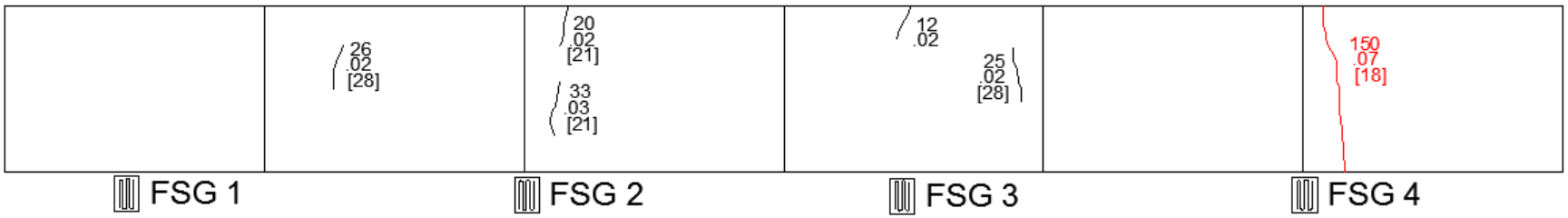

(b)

Figure 4.18 Mix PPE0.20 Crack-maps for (a) Ring 1 and (b) Ring 2

While mix PPE0.20's passing ability fell below our minimum requirements, achieving only a 17 inch J-ring, depending on the individual use, the mix may have some applications. The additional fibers, totaling 0.20% by volume, improved the free shrinkage by almost 9% over the control SCC mix, and improved cracking strain by over 22%. Combined, these two improved properties led to a much improved restrained shrinkage performance.

The first ring sample from this mix showed a steady increase in steel strain up until the 21st day, at which point FSG 1 experienced an immediate loss of strain. The crack-map done on the 22nd day showed a small crack forming between VWSG 1 and VWSG 2. Figure 4.15 shows both of these VWSGs indicate a high tensile stress around the time the cracking was observed, passing the cracking strain threshold on the 22nd day.

Around the time of day 25, VWSG 1 begins to show a large increase in tensile strain, indicating that cracking likely propagated the entire height of the ring at that time. Observation of the paraffin wax layer on the top surface of the ring showed that the crack had expanded and thus the VWSG was no longer measuring concrete strain but the width of the crack, resulting in the large increase in strain.

The 28-day crack-map in Figure 4.18 show that most cracking was centered around VWSG 1 and VWSG 2, while most other regions remained uncracked. Crack width in the first ring, measuring a maximum of 0.06mm, was lower than previous rings as well.

Ring 2 of mix PPE0.20 showed signs of cracking earlier, on day 18 in the FSG sensors. The crack map revealed only one crack on the ring at that time. Strain in the steel steadily increased in the un-cracked portions of the ring until approximately 23 days, at

which point two of the sensors show a quick decrease in compressive strain while two show an increase. Observation of the ring showed the initial crack, shown in red in Figure 4.18b, had reached the steel by day 23.The 28 day crack-map showed, as in ring 1, that cracking outside the single large crack was not as widespread as it was with other mixes. While some cracks appeared in the region surrounding FSG 2 and FSG 3, the high-fiber FR-SCC mixes showed much less cracking overall.

4.5.2.5 Age of Cracking

Among the parameters used to compare the restrained shrinkage is the age of cracking. Ideally, an improved mix will delay the onset of cracking in a restrained shrinkage test. The cracking age, for the purposes of this study, is noted at four different points.

In each of the samples used for this study, the foil strain gauge sensors show a sudden drop in compressive strain in the steel ring. This drop is used as the first indicator that cracking has begun. Alternatively, the VWSGs can be used to determine the development of a crack in the ring. When the strain measured by a VWSG exceeds the cracking strain, cracks should be present in the region of that ring.

Once either the FSG or VWSG sensors indicate a possible crack, the ring is then observed using a digital microscope. If the crack is not yet visible on the surface, the ring is checked daily for the first signs of cracking.

Finally, the cracks observed using the digital microscope are monitored over the remainder of the test. Typically, one major crack becomes apparent, propagating up and down the surface of the ring. As stresses build, the crack propagates inward towards the steel ring at the center of the specimen. The crack depth is checked regularly by eye; once

the crack reaches the ring, a line typically appears through the layer of paraffin wax coating the top surface of the ring. The day on which this line appears is noted as the day the crack has propagated completely.

Table 4.9 Age of First Crack for Restrained Shrinkage Rings

Age of Cracking	PPE0.00		PPE0.10		PPE0.15		PPE0.20	
	R-1	R-2	R-1	R-2	R-1	R-2	R-1	R-2
Age of Cracking (FSG)	13	13	14	15	18	15	22	17
Age of Cracking (VWSG)	13		15		19		22	
First Crack Observed	14	14	16	15	18	16	22	18
Complete Propagation	20	20	22	20	23	21	25	23

Table 4.9 summarizes the various cracking-age measurements taken during the course of the study. What we found was a general trend of increasing cracking age as fiber contents increases.

The highest fiber-volume mix, Mix PPE0.20, took 4-9 day longer to show initial signs of cracking than the control mix. In the context of this study, that is a significant amount of time when considering the free shrinkage of mix PPE0.20 increased by 45 microstrains, or 10% of the 28-day value, during the days 14 to 21.

The duration of time for the crack to propagate inwards, on the other hand, remained the same for all mixes. While the first crack may be delayed in FRSCC mixes, the cracks reached the steel ring within 4-6 days after they first appeared, which is typical of all the mixes used in this study.

The two sensors used on the restrained shrinkage rings, the VWSGs and FSGs, both were found to be accurate in determining the age of cracking in a specific sample. While the VWSGs seem more capable of finding the specific location of a current or

future, their function is limited once a crack opens up. The FSG, however, seem to be better indicators when a crack will happen, often showing a strain jump at the same time, or slightly before, a crack is visible on the surface. The VWSGs on the other hand lag behind slightly; reaching cracking strain just after the crack is detected by the FSG sensors. For optimal timing and measurement, both sensors can be used without adversely affecting the cracking behavior, provided the embedded bolts are of a sufficiently small diameter.

4.5.2.6 Crack Width

Measuring the largest crack width in each sample can be an indicator of the effectiveness of the polypropylene fibers. The digital microscope used for crack observation allowed for precise measuring at 0.005mm intervals. Small crack widths indicate the concrete may retain some strength even after cracking occurs, thereby preventing excessive crack propagation. The crack widths measured are summarized in Table 4.10.

Table 4.10 Crack Widths for Restrained Shrinkage Rings

Crack Width	PPE0.00		PPE0.10		PPE0.15		PPE0.20	
	R-1	R-2	R-1	R-2	R-1	R-2	R-1	R-2
Max crack width (mm)	0.08	0.09	0.08	0.08	0.08	0.08	0.06	0.07

We noticed a decrease in crack width as fiber volume was increased. Average crack width between samples fell from 0.085mm to 0.065mm, or a decrease of 23%. Fibers added into the mix have been found to bridge the gap created by the crack. As a result, a greater force is required for a crack to expand and so crack widths are limited.

4.5.2.7 Tensile Stresses within Rings

Hossain and Weiss' (2004) study on the development of stresses in restrained shrinkage rings described a method by which the tensile stresses in the ring can be determined using the strain gauges described by the AASHTO PP-34 standards. Based on the geometry of the ring and the strain measured in the steel, the equation, described in Equation 2.1 in Section 2.6, is used to determine the tensile stress on the innermost surface of the concrete ring. The results based on this method, as well as the actual tensile strength and the error at the time of cracking are displayed in Table 4.11.

Table 4.11 Tensile Stresses based on Hossain & Weiss' Equation

	PPE 0.00		**PPE 0.10**		**PPE 0.15**		**PPE 0.20**	
	R-1	R-2	R-1	R-2	R-1	R-2	R-1	R-2
Tensile Strength, psi	361		385		398		410	
Tensile Stress, psi	433	385	469	451	493	517	517	535
Percent Error, %	20	7	22	17	24	30	26	30

The errors using this method are high, reaching as high as 30% in the mixes with higher fiber content. The equations being considered assume ideal conditions with a frictionless ring and an even distribution of strain. However, the surface of the steel, while smooth, is not frictionless, especially when the shrinking concrete compresses against the ring. Additionally, the study focused on mortar mixes which have been assumed to shrink evenly. Measures are taken to keep shrinkage even, including the paraffin wax on the top surface and the line of silicone caulk along the bottom, however as the VWSGs show, shrinkage is not even along the circumference of the ring.

Alternatively, tensile stress can be measured within the rings at the location of the embedded vibrating wire strain gauges. Hossain and Weiss (2004) have shown that the

circumferential tensile stress within the ring is reduced towards the outer surface. This is because the total surface area increases as the radius increases, resulting in a larger area around which the stress is applied. This circumferential stress is calculated by multiplying the inner-surface tensile stress by a factor of the inner radius divided by the radius at the point of measurement. This calculated tensile stress can be compared to the measured tensile stress of the vibrating wire gauges at the time of cracking as well as the tensile strength of the concrete cylinder. The measured VWSG stress is found using the maximum value of all VWSGs, as this occurs at the location of the crack. The results are shown in Table 4.12.

Table 4.12 Stress Calculations at VWSGs

Tensile Stress @ VWSG	**PPE 0.00**	**PPE 0.10**	**PPE 0.15**	**PPE 0.20**
Tensile Strength, psi	361	385	398	410
Tensile Stress – Calculated (% of Strength)	347 (96%)	377 (98%)	387 (97%)	424 (103%)
Tensile Stress – Measured (% of Strength)	344 (95%)	361 (94%)	382 (96%)	400 (98%)

We notice that the tensile stresses, both calculated by the Hossain and Weiss (2004) equations and directly measured through the use of vibrating wire gauges are not only approximately equal, but very close to the maximum tensile strength of the concrete cylinder. What this tells us is that it is possible that the concrete has varying mechanical properties within the restrained shrinkage ring. The concrete closer to the steel ring seems to have a higher tensile strength than the concrete located halfway between the steel and the surface. This may be because the outer surface of the ring dries quicker due to surface evaporation, while the inner concrete remains hydrated from residual pore water.

Verifying this would require alternative testing methods; however we can conclude that the VWSGs can accurately represent the concrete conditions at cracking.

4.5.2.8 Cracking Area

An alternative metric used to quantify the extent of cracking throughout the ring is the measurement of cracking area. To calculate the cracking area of a ring sample, the length and width of all cracks are measured through the digital microscope described earlier and the area of all the cracks is summed. Unlike the maximum crack width measurement, the cracking area gives us a better understanding of the extent of cracking throughout the ring rather than at one specific point. For FRSCC, this is especially important because fibers may cause smaller, more closely dispersed, cracks as opposed to a single large crack.

Table 4.13 Cracking Area for Restrained Shrinkage Rings

	PPE 0.00		**PPE 0.10**		**PPE 0.15**		**PPE 0.20**	
	R-1	R-2	R-1	R-2	R-1	R-2	R-1	R-2
Cracking Area, mm^2	19.1	20.0	16.8	17.3	15.5	15.4	12.7	13.1

The results of the cracking area measurements are summarized in Table 4.13. It is apparent that the cracking area drops noticeably with even the smallest addition of fibers tested in this study. Even as the maximum crack width remained unchanged from PPE 0.10 to PPE 0.15, the cracking area falls with the small addition of fibers from an average of 17.1 mm^2 to 15.5mm^2. In total, the average cracking area falls over 34% over the control mix when fibers are added at 0.20% by volume.

CHAPTER V

5 SUMMARY AND CONCLUSIONS

5.1 CONCLUSIONS

This study aimed to analyze the cracking behavior of a set of SCC mixes with varying amounts of polypropylene fibers. The mix design focused on creating an economical, workable, FRSCC mix with improved physical properties. For this reason, slag cement was used as a partial replacement for Portland cement. Additionally, keeping cement content low, to 675 pounds per cubic yard, helps keep bulk cost down for the mix. Once the mix design was decided upon, three main parameters were tested for this set of mixes: (1) the wet concrete properties including workability, passing ability and air content, (2) the strength characteristics and (3) the shrinkage properties, including the free and restrained shrinkage.

Based on the results gathered from this study, the following conclusions can be made: the inclusion of polypropylene fibers negatively affects concrete workability and, to a greater extent, concrete passing ability. Since concrete flowing properties are highly dependent on the cementitious content, a low-paste mix, such as the one used in this study, is extremely susceptible to extreme loss of passing ability, even when water-reducers are used. In this study, for example, we found the J-ring flow to be reduced by

5.5 in, or 24%, when fibers were added at 0.20%, while the slump was only reduced by 1.5 in, or 6%.

In the specific case of the mix proportions used in this study, the maximum allowable fiber volume should be kept at 0.15% to maintain workability and passing ability requirements for a mix containing 675lb of cement per cubic yard. Beyond this, L-box and J-ring tests will reflect a significant loss in passing ability and consolidation issues may occur. Higher fiber contents may be possible when cementitious content is increased.

Mechanical properties of the concrete are impacted by the fiber content. Compressive strength, for example, shows a small rise as fiber content is increased; gaining 9% when fiber is added at 0.20%. Tensile splitting strength shows a more significant gain, increasing by over 13% over the control SCC mix. Elastic modulus, on the other hand, shows a small decrease as fibers are added, falling by 7% when fibers are added at 0.20% by volume.

Free shrinkage strain was reduced as fiber content was increased, with 28-day free shrinkage measurements showing a reduction of 4%, 8% and 9% for fiber volumes of 0.10%, 0.15% and 0.20%. While the improvement is small, mostly due to the small range of fiber volume being tested, studies suggest this trend would continue as fiber contents were increased further.

Concrete performance under restrained shrinkage conditions was also improved as fiber content was increased. Initial cracking was delayed in the FRSCC restrained shrinkage ring samples. While the control SCC mix had visible cracking on the surface of both samples at 14 days after casting, the mix with 0.10% fiber by volume cracked, on

average, 15.5 days after casting. Increasing the fiber content to 0.15% by volume resulted in cracking at 17 days after cracking, while the highest fiber content, 0.20% by volume, cracked, on average, 20 days after casting.

FRSCC mixes in this study were found to have smaller cracks at the end of the testing period. While all samples had cracked by 28 days, the control SCC mix had the largest maximum crack width, measuring on average to be 0.085mm wide. With fibers added at 0.10% by volume, the maximum crack width was measured at 0.08mm. Further increasing fibers to 0.15% by volume kept crack width at 0.08mm, while the mix containing 0.20% fibers by volume had an average maximum crack width of 0.065mm. The smaller crack size is an indication that the fibers maintained strength even as the concrete fractured; holding the crack together.

Vibrating wire strain gauges (VWSGs) were added to the restrained shrinkage test to supplement the data being gathered from the foil strain gauges (FSGs) in the steel. The study found that the FSGs, currently part of the AASHTO PP-34 standards, can be supplemented with VWSGs to more accurately identify cracking and stress development within the concrete.

While the FSGs are useful in telling us when cracking has occurred, the VWSGs give us an indication of which regions of the ring are developing higher tensile stresses. As a result, with the VWSGs, we can predict where a crack will occur based on the stresses in the six sensors. If a ring remains un-cracked after the test has concluded, the VWSGs can also give us an idea of how close the ring was to being cracked at the conclusion of the test.

However, even with the VWSGs, the FSGs are necessary for the test because the study found that the cracking originates from the interface between the steel and the concrete. As a result, the FSG sensors are the first to react when a microcrack has developed. Sometime later, the VWSGs in the region of the crack pass the cracking strain threshold and sometime after that the crack appears on the surface of the ring.

Results indicate that the sealing method used in this experiment may cause uneven drying during the early stages of the test. Water needs to permeate to the surface which may take time, resulting in a greater degree of curing on the inner concrete than the surface concrete. As a result, mechanical properties may vary within the concrete ring and skew cracking age results.

While the section loss due to the embedded bolts did not have a measurable effect the age of cracking or the maximum measured tensile stresses, the cracking pattern indicated that shrinkage cracks occur near the location of the embedded bolts. However small, the section loss may influence the cracking behavior in restrained shrinkage rings.

5.2 SCOPE FOR FUTURE RESEARCH

This study focused on a small subset of SCC mixes, prioritizing an economically viable mix by using a high slag content and low cementitious weight. Future studies on restrained shrinkage can be done using mixes with a higher overall cementitious content. A higher paste volume will allow for a greater range of fiber volume to be experimented with without falling below the workability and passing ability thresholds.

Alternatively, other cementitious materials can be tested instead of blast furnace slag. Silica fume, though more of an additive than a substitute, can be used in SCC mixes.

The addition of silica fume, a material often used in high performance concrete (HPC), to a concrete mix will improve physical properties of the concrete and will likely have an effect on the shrinkage behavior. Fly ash, another cementitious material, can also be added as a substitute for Portland cement. Low cost and pozzolanic properties make fly ash a popular additive in concrete.

A greater variety of admixtures may allow more flexibility in terms of mix design. For the purposes of this study, only a high-range water reducer (HRWR) was used to assist in the workability and passing ability tests. However, when added in larger amounts, HRWRs tend to create segregation within the mix. Too much HRWR will lead to excessive bleeding and the subsequent mix will be unsuitable. Viscosity modifying admixtures can be used to prevent bleeding and segregation and, possibly, allow for higher fiber volumes to be used with the same mix proportions.

The curing conditions for this study were kept to a one day wet cure to conform to the AASHTO PP-34 standards. A longer curing time would delay or prevent cracking from occurring, but would also be more indicative of on-site concrete conditions. Agency specific standards dictate concrete curing time and curing procedure, which can vary from state to state. Extending the curing time would also extend the testing period of the tests, likely requiring shrinkage monitoring to continue past 56 days.

The VWSG sensors used in this study had no apparent effect on stress development, however cracking in the restrained shrinkage rings tended to occur at the points the bolts were embedded. Utilizing a smaller bolt diameter may further minimize this effect while still providing the useful information gathered from direct strain measurements.

REFERENCES

1. B. Shindman and D. Panesar, "Comparative study of plastic property test methods for self-consolidating concrete," *Canadian Journal of Civil Engineering,* pp. 937-950, 2012.

2. A. Leemann, P. Nygaard and P. Lura, "Impact of Admixtures on the Plastic Shrinkage Cracking of Self-Compacting Concrete," *Cement & Concrete Composites,* pp. 1-7, 2014.

3. M. Barfield and N. Ghafoori, "Air-entrained self-consolidating concrete: A study of admixture sources," *Construction and Building Materials,* pp. 490-496, 2012.

4. W. Nocun-Wczelic, T. Wasag, M. Stycynska and G. Miklaszewski, "Effect of some concrete admiztures on the portland cement hydration," *Cement Wapno Beton,* pp. 223-231, 2009.

5. L. Du and K. Folliard, "Mechanisms of air entrainment in concrete," *Cement and Concrete Research,* pp. 1463-71, 2005.

6. B. Lazniewska-Pierkarczyk, "The influence of chemical admixtures on cement hydration and mixture properties of very high performance self-compacting concrete," *Construction and Building Materials,* pp. 643-662, 2013.

7. N. Rajamane, J. Annie Peter, J. Dattatreya, M. Neelamegam and S. Gopalakrishnan, "Improvement in properties of high performance concrete with partial replacement of cement by ground granulated blast furnace slag," *Journal of the Institution of Engineers. India. Civil Engineering Division,* pp. 38-42, 2003.

8. G. Osborne, "Durability of Portland blast-furnace slag cement concrete," *Cement and Concrete Composites,* pp. 11-21, 1999.

9. K. Khayat, "Workability, Testing, and Performance of Self-Consolidating Concrete," *ACI Material Journal,* pp. 346-354, 1999.

10. R. Loser and A. Leeman, "Shrinkage and restrained shrinkage cracking of self-compacting concrete compared to conventionally vibrated concrete," *Materials and Structures,* pp. 42-71, 2009.

11. P. Turcry, A. Loukili, K. Haidar, G. Pijaudier-Cabot and A. Belarbi, "Cracking Tendency of Self-Compacting Concrtete Subjected to Restrained Shrinkage:

Experimental Study and Modeling," *Journal of Materials in Civil Engineering,* vol. 18, no. 1, pp. 46-54, 2006.

12. S. N. Tande and P. B. Mohite, "Applications of Self Compacting Concrete," in *Our World in Concrete & Structures,* Singapore, 2007.

13. H. Shah and J. Weiss, "Quantifying Shrinkage Cracking in Fiber Reinforced Concrete using the Ring Test," *Materials and Structures,* vol. 39, pp. 887-899, 2006.

14. D. Saje, B. Bandeji, J. Sustersic, J. Lopatic and F. Saje, "Shrinkage of Polypropylene Fiber-Reinforced High-Performance Concrete," *Journal of Materials in Civil Engineering,* vol. 23, no. 7, pp. 941-952, 2011.

15. H. Okamura and M. Ouchi, "Self-Compacting Concrete," *Journal of Advanced Concrete Technology,* pp. 5-15, 2003.

16. H. Okamura, K. Maekawa and K. Ozawa, "High-Performance Concrete," *Gihido Publishing,* 1993.

17. S.-H. Kwon, R. P. Ferron, Y. Akkaya and S. Shah, "Cracking of Fiber-Reinforced Self-Compacting Concrete Due to Restrained Shrinkage," *International Journal of Concrete Structures and Materials,* vol. 1, no. 1, pp. 3-9, 2007.

18. A. Hossain and J. Weiss, "Assessing Risidual Stress Development and Stress Relaxation in Restrained Concrete Ring Specimens," *Cement & Concrete Composites,* vol. 26, pp. 531-540, 2004.

19. O. Gencel, C. Ozel, W. Brostow and G. Martinez-Barrera, "Mechanical Properties of Self-Compacting Concrete Reinforced with Polypropylene Fibers," *Materials Research Innovations,* vol. 15, no. 3, pp. 216-225, 2011.

20. A. El-Dieb and M. R. Taha, "Flow Characteristics and Acceptance Criteria of Fiber-Reinforced Self-Compaced Concrete (FR-SCC)," *Construction and Building Materials,* vol. 27, pp. 585-596, 2012.

21. M. C. Brown, C. Ozyildirim and W. Duke, "Investigation of Fiber-Reinforced Self-Consolidating Concrete," Virginia Transportation Research Council, Charlottesville,Va, 2010.

22. V. Dao, P. Dux, P. Morris and L. O'Moore, "Plastic Shrinkage Cracking of Concrete," *Australian Journal of Structural Engineering,* pp. 210-214, 2010.

23. J. Mora-Ruacho, R. Gettu and A. Aguado, "Influence of shrinkage-reducing admixture on the reduction of plastic shrinkage cracking in concrete," *Cement and Concrete Reasearch,* pp. 141-146, 2009.

24. S. Mindess, J. F. Young and D. Darwin, Concrete, 2nd ed, Upper Saddle River, NJ: Pearson Education, Inc., 2002.

25. B. Klemczak and A. Knoppik-Wrobel, "Analysis of Early-Age Thermal and Shrinkage Stresses in Reinforced Concrete Walls," *ACI STRUCTURAL JOURNAL,* pp. 313-322, 2014.

26. A. Osipov, "Concrete Setting Retarders," *Hydrotechnical Construction,* pp. 670-678, 1976.

27. D. Cusson and T. Hoogeveen, "Internal curing of high-performance concrete with pre-soaked fine lightweight aggregate for prevention of autogenous shrinkage cracking," *Cement and Concrete Research,* pp. 757-765, 2007.

28. E.-i. Tazawa and S. Miyazawa, "Influence of Cement and Admixture on Autogenous Shrinkage of Cement Paste," *Cement and Concrete Research,* pp. 281-287, 1995.

29. E.-i. Tazawa and S. Miyazawa, "Experimental Study on Mechanism of Autogenoush Shrinkage of Concrete," *Cement and Concrete Research,* pp. 1633-1638, 1995.

30. N. Gardner, "Comparison of prediction provisions for drying shrinkage and creep of normal-strength concretes," *Canadian Journal of Civil Engineering,* pp. 767-775, 2004.

31. F. Collins and S. J.G., "Effect of pore size distribution on drying shrinkage of alkali-activated slag concrete," *Cement and Concrete Research,* pp. 1401-1406, 2000.

32. J. Romualdi and J. Mandel, "Tensile Strength of Concrete Affected by Uniformly Distributed and Closely Spaced Short Lengths of Wire Reinforcement," *Journal of the American Concrete Institute,* pp. 657-671, 1964.

33. R. Zollo, "Fiber-reinforced Concrete: an Overview after 30 Years of Development," *Cement and Concrete Composites,* pp. 107-122, 1997.

34. N. Banthia and R. Gupta, "Influence of polypropylene fiber geometry on plastic shrinkage cracking in concrete," *Cement and Concrete Research,* pp. 1263-1267, 2006.

35. F. Aslani and B. Samali, "High Strength Polypropylene Fibre Reinforcement Concrete at High Temperature," *Fire Technology,* pp. 1229-1247, 2014.

36. H. Mazaheripour, S. Ghanbarpour, S. Mirmoradi and I. Hosseinpour, "The effect of polypropylene fibers on the properties of fresh and hardened lightweight self-compacting concrete," *Construction and Building Materials,* pp. 351-358, 2011.

37. E.-i. Tazawa, S. Miyazawa and T. Kasai, "Chemical Shrinkage and Autogeneoush

Shrinkage of Hydrating Cement Paste," *Cement and Concrete Research,* pp. 288-292, 1995.

38. W. Yodsudjai and K. Wang, "Chemical shrinkage behavior of pastes made with different types of cements," *Construction and Building Materials,* pp. 854-862, 2013.

39. D. Whiting, R. Detwiler and E. Lagergen, "Cracking tendency and drying shrinkage of silica fume concrete for bridge deck applications," *ACI Structural Journal,* pp. 71-77, 2000.

40. D. Roy, "Alkali-activated cements: opportunities and challenges," *Cement and Concrete Research,* pp. 249-254, 1999.

41. T. Kanda, H. Momose, K. Yoda, K. Imamoto and A. Ogawa, "Experimental study of blast-Furnace slag blended cement concrete investigating and improving shrinkage cracking resistance," *Journal of Structural and Construction Engineering,* pp. 9-18, 2014.

42. A. Melo Neto, M. Cincotto and W. Repette, "Drying and autogenous shrinkage of pastes and mortars with activated slag cement," *Cement and Concrete Research,* pp. 565-574, 2008.

43. N. Eldin and A. Senouci, "Rubber-Tire Particles as Concrete Aggregate," *Journal of Materials in Civil Engineering,* pp. 478-496, 1993.

44. R. Carlson, "DRYING SHRINKAGE OF CONCRETE AS AFFECTED BY MANY FACTORS," *Transportation Research Board,* pp. 419-437, 1938.

45. P. Klieger and J. Lamond, "Significance of Tests and Properties of Concrete and Concrete-making Materials," *ASTM STP 196C,* p. 610, 1994.

46. A. Bentur, S. Igarashi and K. Kovler, "Prevention of autogenous shrinkage in high-strength concrete by internal curing using wet lightweight aggregates," *Cement and Concrete Research,* pp. 1587-1591, 2001.

47. S. H. Kosmatka and M. L. Wilson, Design and Control of Concrete Mixtures, Washington DC: Portland Cement Association, 2011.

48. H. Qin, Z. Fei, W. Guo and Q. Tian, "The effects of water-reducer on early-age plastic shrinkage of concrete," *Applied Mechanics and Materials,* pp. 1113-1118, 2012.

49. K. B. N. Folliard, "Properties of High-performance Concrete Containing Shrinkage Reducing Admixtures," *Cement and Concrete Research,* pp. 1357-1364, 1997.

50. S. Shah, Fiber Reinforced Concretes - A review of capabilities, The Aberdeen Group,

1981.

51. P. Song, S. Hwang and B. Sheu, "Strength Properties of Nylon- and Polypropylene-fiber-reinforced concretes," *Cement and Concrete Research*, pp. 1546-1550, 2004.

52. I. Chu, S. Kwon, M. Amin and J. Kim, "Estimation of temperature effects on autogenous shrinkage of concrete by a new prediction model," *Construction and Building Materials,* pp. 171-182, 2012.

53. X.-Q. Qian, T. Meng, S.-L. Zhan and K.-L. Qian, "Influence of relative humidity on shrinkage of mortar and concrete," *Journal of Shenyang Jianzhu University,* pp. 268-271, 2006.